Theoretical Studies of the Structure and Bonding of Actinide Complexes

B. E. Bursten[*,†], J. Li[#], T. Yang[†], J. L. Sonnenberg[†], and M. Mrozik[†]

[*]Department of Chemistry, University of Tennessee, Knoxville TN 37902 USA
[†]Department of Chemistry, The Ohio State University, Columbus OH 43210 USA
[#]William R. Wiley Environmental Molecular Sciences Laboratory, Pacific Northwest National Laboratory, Richland WA 99352 USA

We have used density functional theory with relativistic corrections and higher level electronic structural methodologies to address the structure and bonding of a number of interesting actinide coordination complexes. Results will be presented on a variety of systems, including the products of laser-ablated actinide atoms with small substrate molecules, coordination complexes of actinide and actinyl ions with unusual ligands, and the multi-shell coordination chemistry of actinide ion in aqueous solution.

Among the specific systems to be discussed will be the CUO molecule, which is formed experimentally upon the reaction of U atoms with CO and which shows significant interactions with noble-gas atoms. We will recap the history of the discovery of this unusual bonding interaction, which has ultimately led to unusually extensive noble-gas coordination chemistry at a uranium center. These results will be extended to a discussion of molecular UO_2, which has received a great deal of recent experimental and theoretical study and has proven to be a vexing molecule with respect to electronic structure.

We will also present recent results on using density functional theory to describe the static structures of the first two hydration shells of the hydrated Cm^{3+} ion (Figure 1).   We have used molecular dynamics calculations to determine the lifetime of the second shell, which we predict to be stable enough to be observed.
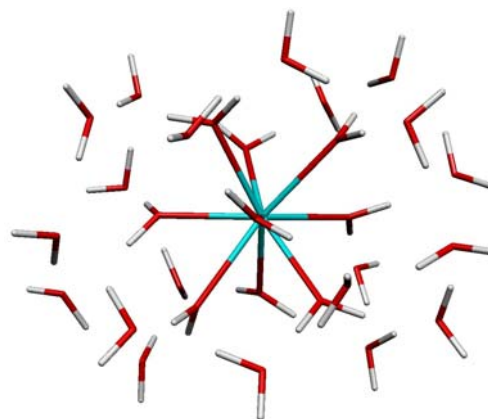

Fig 1: Depiction of the optimized structure of a Cm^{3+} ion with nine and 20 water molecules in the first and second coordination spheres: $[Cm(H_2O)_9(H_2O)_{20}]^{3+}$

Finally, we will present our recent studies of unusual structural motifs, including bent uranyl complexes and organouranium complexes that contain "linear" Cp*-U-Cp* (Cp* = η^5-C_5Me_5) linkages.

Fun at the Bottom of the Periodic Table: Novel Reactivity Patterns in Actinide Molecular Systems

Jaqueline L. Kiplinger

Los Alamos National Laboratory, Los Alamos NM 87545 USA

Although transition-metal complexes possessing terminal Schrock-type alkylidene $(M=CR_1R_2)$ functionalities are well known, related actinide complexes have remained elusive.[1] Traditional routes employed for the preparation of transition-metal alkylidene complexes include α-hydrogen abstraction and carbene transfer from diazoalkanes.[1]

We have investigated the reaction chemistry of low-valent organouranium complexes with diazoalkanes. Reaction of the known complex $(C_5Me_5)_2UCl_2$ with two reducing equivalents (provided by KC_8), followed by reaction with excess diphenyldiazomethane generates the bis(diphenyldiazomethane) uranium complex $(C_5Me_5)_2U(=N-N=CPh_2)(\eta^2-(N_2)-N=N=CPh_2)$ (Figure 1).
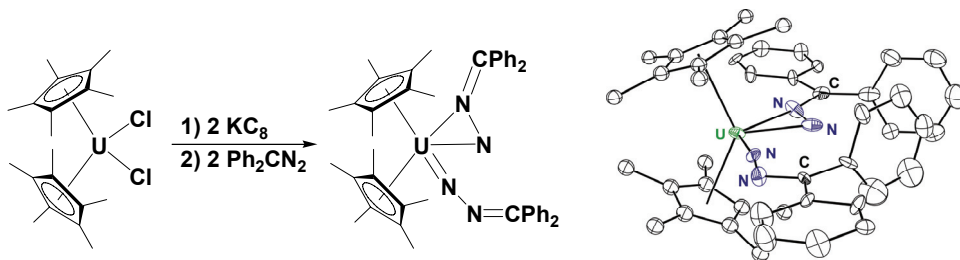

Fig 1: Synthetic scheme for the preparation of a uranium diazoalkane complex and its molecular structure.

This is the first example of a diazoalkane actinide complex and is unlike existing transition metal diazoalkane complexes in that it possesses two diazoalkane molecules bound to a single uranium metal center: one diazoalkane is coordinated to the uranium metal center in an η^1-fashion and forms a uranium imido (U=N) bond with a short U−N bond distance of 1.921 Å and a U−N−N bond angle of 172.8°. The second diazoalkane is coordinated to the uranium in an η^2-manner, possibly through the N=N π-system (U−N = 2.452, 2.325 Å). The exceedingly long N−N bond distance (1.411 Å) compared with that of uncomplexed diazoalkanes (1.12–1.13 Å) indicates that substantial π-backbonding from the $(C_5Me_5)_2U$ fragment (orbitals of the appropriate symmetry exist) to the diazoalkane lowest unoccupied molecular orbital (LUMO), which is N−N antibonding. Interestingly, theoretical (DFT) calculations reveal an $f^1\pi^*$ electronic configuration and suggest delocalization of a 5f electron throughout the N=N=C framework of the η^2-coordinated diazoalkane. Spectroscopic data support the hypothesis of donation of electron density from the uranium metal center onto the diazoalkane molecule.

Recent reports have shown that oxidatively induced α-hydrogen abstraction may be used to prepare early transition metal alkylidene complexes.[2] The propensity of uranium to exist in the

hexavalent oxidation state coupled with the known oxophilicity of tetravalent uranium, suggested to us that uranium(VI) alkylidene complexes of the type, $(C_5Me_5)_2U(=O)(=CHR)$, might be prepared by oxidatively-induced α-hydrogen abstraction chemistry between uranium(IV) bis(alkyl) complexes such as $(C_5Me_5)_2U(CH_2R)_2$ and an appropriate oxygen atom transfer agent.

Pyridine N-oxide is a prototypical oxygen atom transfer reagent that has been routinely used in the synthesis of high-valent transition metal and actinide oxo complexes.[3] We have found that uranium(IV) and thorium(IV) bis(alkyl) complexes of the type $(C_5Me_5)_2AnR_2$ (An = U, Th; R = CH_3, CH_2Ph) instead activate the sp^2 and sp^3 hybridized C-H bonds in pyridine N-oxide and lutidine N-oxide to produce the corresponding cyclometallated complexes, $(C_5Me_5)_2An(R)[\eta^2$-(O,C)-$ONC_5H_4]$ and $(C_5Me_5)_2An(R)[\eta^2$-(O,C)-ON-2-CH_2-5-CH_3-$C_5H_3]$ (Figure 2).[4]
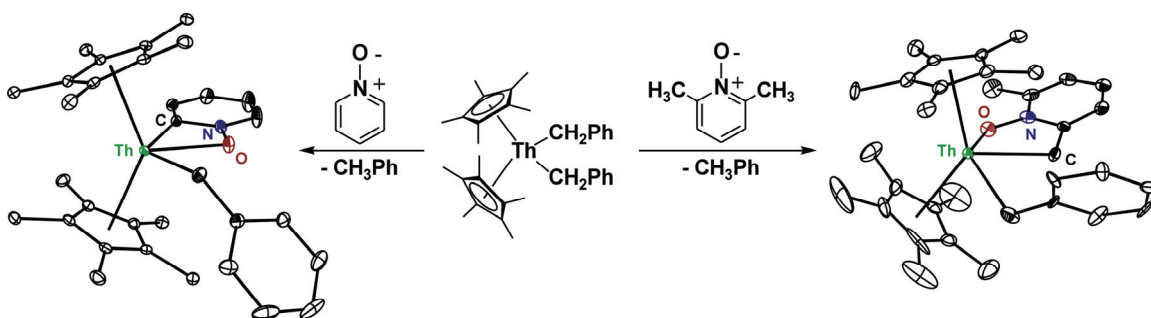

Fig 2: Scheme illustrating the reactivity of $(C_5Me_5)_2Th(CH_2Ph)_2$ towards sp^2 and sp^3 hybridized C-H bonds in pyridine N-oxides.

Interestingly, the thorium(IV) bis(alkyl) and bis(aryl) complexes $(C_5Me_5)_2ThR_2$ (Me = CH_3, R = $CH_2C_6H_5$ or C_6H_5) have been found to mediate ring-opening and dearomatization of the pyridine ring in pyridine N-oxide under ambient conditions to afford the first thorium η^2-(O,N) oximate complexes.[5] These reactions provide rare examples of C–H and C=N activation chemistry mediated by actinide metal ions with accessible 5f orbitals, and such transformations represent new types of reactivity available to pyridine N-oxide. Recent developments in this exciting area of chemistry will be presented.

1   R. R. Schrock, Chem. Rev. **102**, 145-179 (2002), and references therein.
2   F. Basuli, B. C. Bailey, J. Tomaszewski, J. C. Huffman, and D. J. Mindiola, J. Am. Chem. Soc. **125**, 6052-6053 (2003).
3   For example, see: (a) C. C. Cummins, R. R. Schrock, and W. M. Davis, Inorg. Chem. **33**, 1448-1457 (1994). (b) S. M. Mullins, A. P. Duncan, R. G. Bergman, and J. Arnold, Inorg. Chem. **40**, 6952-6963 (2001). (c) K. M. Sung, and R. H. Holm, J. Am .Chem. Soc. **123**, 1931-1943 (2001).
4   J. A. Pool, B. L. Scott, and J. L. Kiplinger, J. Am. Chem. Soc. **127**, 1338-1339 (2005).
5   J. A. Pool, B. L. Scott, and J. L. Kiplinger, Chem. Commun. 2591-2593 (2005).

Covalency in the *f*-element–chalcogen bond. Computational studies of [M(N(EPR$_2$)$_2$)$_3$] (M = Pu, U, Ce, La; E = O, S, Se, Te; R = H, Me)

K. I. M. Ingram[*], N. Kaltsoyannis[*], A. J. Gaunt[†], M. P. Neu[†]

[*] University College London, London, WC1H 0AJ, UK.
[†] Los Alamos National Laboratory, Los Alamos, NM 87545, USA.

INTRODUCTION

Current understanding of chemical bonding involving 5*f*-elements still trails behind that of the transition metals and lanthanides. This is partly due to a paucity of well characterized molecular complexes featuring donor atoms spanning the range from hard to soft, as actinide chemistry has traditionally been dominated by hard donor ligands, especially oxygen. Recently, however, there has been increased research into the chemistry of the actinides with softer donor ligands such as nitrogen and sulfur. This interest is partly fundamental, but also stems from the anticipation that subtle differences between lanthanide 5*d*4*f*- and actinide 6*d*5*f*-orbital bonding with soft donor ligands will find application in the separation of lanthanides from actinides in, for example, nuclear wastes.[1] A thorough understanding of the changes in *f*-element–ligand bonding as the donors progress from hard to soft, especially the extent to which covalent interactions influence chemical structure and reactivity, is therefore extremely important for both fundamental and applied reasons.

At the *Actinides 2005* conference in Manchester, UK, and in reference 2, two of us reported the synthesis and characterisation of a range of homoleptic, trivalent lanthanum and uranium complexes with imidodiphosphinochalcogenide ligands [N(EPPh$_2$)$_2$]$^-$ and [N(EP^{i}Pr$_2$)$_2$]$^-$ (E = S, Se). The X-ray crystal structure of [U(N(SP^{i}Pr$_2$)$_2$)$_3$] is shown in Figure 1.

The comparison between analogous La(III) and U(III) imidodiphosphinochalcogenide compounds is very interesting for, as shown in Table 1 below, the metal–chalcogen distances show significant differences. Clearly, the U–chalcogen distance in both types of system is significantly shorter than the corresponding La–chalcogen bond, and this difference increases as the chalcogen becomes softer.

Fig 1: The X-ray crystal structure of [U(N(SP^{i}Pr$_2$)$_2$)$_3$].

Given that the six-coordinate ionic radii of La^{3+} and U^{3+} are essentially the same, 1.045 and 1.040 Å respectively, the logical conclusion is that there is some additional bonding interaction present in the uranium compounds, presumably covalent in nature.

Building on the La(III)/U(III) results, very recent work at Los Alamos has furnished analogous Pu(III) and Ce(III) imidodiphosphinochalcogenide complexes (the six co-ordinate
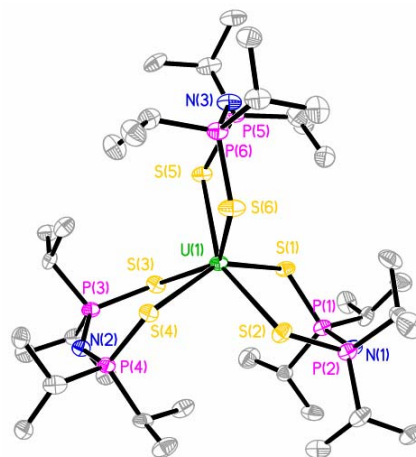
ionic radii of Pu^{3+} and Ce^{3+} are essentially the same as one another). These results allow further An(III)/Ln(III) comparisons to be made, and also comparisons within the actinide and lanthanide series. These new compounds, and the La(III) and U(III) systems discussed above, are the focus of the present computational study, together with complexes containing oxygen- and tellurium-donor imidodiphosphinochalcogenide ligands. The extension to the O- and Te-based ligands allows us to probe the *f*-element–chalcogen bond for all of the first four group 16 elements, with the aim of establishing the extent of covalency, and its dependence upon the metal and chalcogen.

Compound	Bond	Distance/Å	Difference (La-U/Å)
$[La(N(SPPh_2)_2)_3]$	La(III)–S	3.0214(11)	
$[U(N(SPPh_2)_2)_3]$	U(III)–S	2.9956(5)	0.0258
$[La(N(SePPh_2)_2)_3]$	La(III)–Se	3.1229(3)	
$[U(N(SePPh_2)_2)_3]$	U(III)–Se	3.0869(4)	0.0360
$[La(N(SP^iPr_2)_2)_3]$	La(III)–S	2.892(1)	
$[U(N(SP^iPr_2)_2)_3]$	U(III)–S	2.854(7)	0.038
$[La(N(SeP^iPr_2)_2)_3]$	La(III)–Se	3.019(3)	
$[U(N(SeP^iPr_2)_2)_3]$	U(III)–Se	2.964(7)	0.055

Table 1: Metal–ligand bond distances in $[M(N(EPR_2)_2)_3]$ (M = La, U; E = S, Se; R = Ph, ^iPr).

COMPUTATIONAL STUDIES

Relativistic, gradient-corrected density functional theory has been used to probe the geometric and electronic structures of the title compounds (models for the experimentally reported systems). Excellent agreement has been found between the computed geometries and those of the experimentally characterised compounds. The bonding between the metals and the chalcogens has been investigated using a variety of analysis tools, including the Mulliken and NBO population and charge schemes, and the Ziegler-Rauk energy decomposition scheme. It will be shown that the computational data clearly indicate that there are greater covalent interactions between a given metal and the chalcogen donor atoms of the ligands as the chalcogen is altered from O to Te, and also as the metal is changed from Ln to An for a given chalcogen. The relative role of the *d* and *f* valence atomic orbitals in these covalent interactions will be discussed, as will the effects of the actinide contraction, *i.e.* the differences between analogous Pu(III) and Ce(III) complexes will be compared with the corresponding U(III) and La(III) systems.

1   M. P. Jensen and A. H. Bond, J. Am. Chem. Soc. **124(33)**, 9870 (2002).
2   A. J. Gaunt, B. L. Scott and M. P. Neu, Chem. Commun., 3215 (2005).

Soft X-ray Emission and Absorption Spectroscopy for Curium-Nitrogen Donor Ligand Complex System

T. Yaita[*] and D.K. Shuh[**]

[*]Actinide Coordination Chemistry Group, Quantum Beam Science Directorate, Japan Atomic Energy Agency (JAEA), 1-1-1 Koto, Sayo-cho, Sayo-gun, Hyogo 679-5148, Japan.
[**]Actinide Chemistry Group, Chemical Sciences Division, Lawrence Berkeley National Laboratory (LBNL), Berkeley CA 94720-8175, USA.

INTRODUCTION

Soft donor aromatic nitrogen ligands (N-donor) often show unique properties, which are not observed in the oxygen (O)-donor type ligand complexes, in their chemical bonding with trivalent actinides. This unique feature is not observed strongly in lanthanide complexes. Therefore, the application of N-donor ligands have great promise for the partitioning of trivalent actinides from lanthanides for the transmutation of poisonous nuclides such as Am-241 by burning up with an ADS (Accelerator Driven System) or FBR (Fast Breeder Reactor system). This essential mechanism is considered to originate from a covalent interaction between the actinide and ligand, however, no detailed studies on their chemical bond from the viewpoint of electronic structure have been performed to date. In this study, we investigate the valence electronic structure for a Cm-N donor ligand utilizing soft x-ray emission and x-ray absorption spectroscopies. The x-ray emission and

Fig. 1: *1,10*-Phenanthroline (Phen) and the derivatives.

[*]D_M: Distribution ratio of a metal, M; SF= D_{Am}/D_{Eu}.
[**]These extractions were performed by $CHCl_3$ with NH_4SCN under pH=4.

absorption spectra experimentally give us an approximate partial density of state (PDOS). The soft donor ligands in this study are *1,10*-Phenanthroline (Phen) and the derivatives, and show high separation factor between trivalent actinide and lanthanide (SF=D_{Am}/D_{Eu}, D: Distribution ratio), as shown in Fig. 1. The base Phen ligand shows an interesting substituent effect on the SF (Fig. 1) and series of studies on the electronic structure with varying SF would be of particular interest.
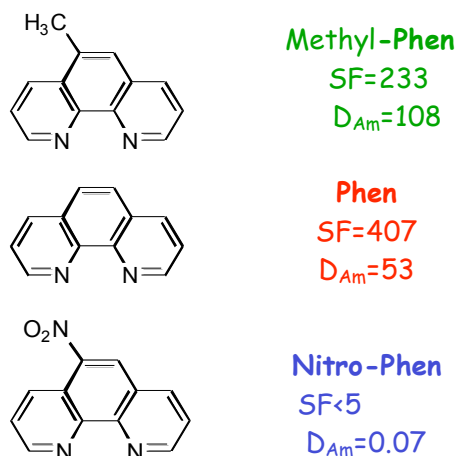
EXPERIMENTAL

Complex samples were synthesized by mixing M^{3+} and ligand with a 1:2 ratio in methanol solutions. In methanol solutions, we have previously confirmed that the trivalent metal ion forms a 1:2 complex with the ligands based on UV-VIS spectrophotometric titration spectra. The x-ray emission and absorption spectra of Cm, Eu and the other lanthanides-ligand complexes were measured at the BLs 7.0.1 and 8.0.1 of the Advanced Light Source. EXAFS structural studies of the lanthanide complexes by were also performed at the BL11 of Super Photon Ring 8 GeV (SPring8).

RESULTS AND DISCUSSION

Figure 2 shows the N-*K* XAS and XES spectra of the Phen, Cm-Phen, and Eu-Phen complexes. All of the spectra corresponding to the ligand 2p PDOS are observed, in which both Fermi levels are located at ~395 eV, measured from N 1s core level. The sharp peaks in the XAS spectra arise from the $1s \rightarrow \pi^*$ transition and are observed within ~1.5eV of $E\text{-}E_F$. The lineshapes of Cm-Phen complex have quite different profiles which exhibit broadening and decreased intensities compared to the Phen ligand when normalized to the peaks for the $1s \rightarrow \sigma^*$ transition at 7~12 eV. The lineshapes of the Eu-Phen spectra do not show appreciable differences compared to the spectra from base ligand. Furthermore, a significant difference in the XES (PDOS of the occupied states) of Cm-Phen spectrum appears around -6 eV (arrow in Fig. 2). It is a noteworthy result from the viewpoint of evidence for a covalent interaction between Cm and Phen ligand. Namely, it suggests that some interaction like back-donation from Cm increases the N-2p PDOS of the Phen. In this presentation, we will discuss the substituent effect in the Phen system and the molecular design of N-donor ligands for 4f/5f separations based on the results of this study.
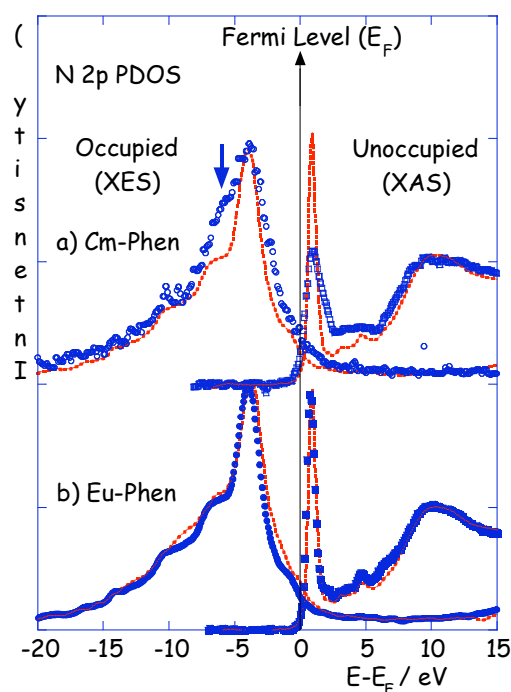
Fig.2:
The experimental N-2p PDOS for the Phen, Cm-Phen, and Eu-Phen derived from XES and XAS spectroscopies.
*The samples are: a) Cm(Phen)$_2$Cl$_3$(H$_2$O)$_x$ (○:XES, □:XAS); b) Eu(Phen)$_2$Cl$_3$(H$_2$O)$_x$ (●:XES, ■:XAS).
** The Phen spectra are overlapped as the dashed line (---).
*** The XES spectra are obtained by x-ray irradiation at greater than 425 eV.

Muon Spin Relaxation (μSR) Studies of α-Pu, δ-Pu and PuCoGa$_5$

R. H. Heffner[a,b], G. D. Morris[c], M. J. Fluss[d], E. D. Bauer[b], B. Chung[d], W. Higemoto[a], T. U. Ito[f], D. E. MacLaughlin[e], S. McCall[d], K. Ohishi[a], J. L. Sarrao[b] and L. Shu[e]

[a] Japan Atomic Energy Agency, Tokai-Mura, Ibaraki-Ken, 319-1195 Japan
[b] Los Alamos National Laboratory, MS K764, Los Alamos, New Mexico 87545 USA
[c] TRIUMF, 4004 Wesbrook Mall, Vancouver, B.C., Canada V6T 2A3
[d] Lawrence Livermore National Laboratory, Livermore, California 94552 USA
[e] Department of Physics, University of California, Riverside, California 92521 USA
[f] Department of Physics, Tokyo Institute of Technology, Meguro-ku, Tokyo 152-8551 Japan

During the past decade there has been a resurgence of interest in the electronic properties of Pu metal and Pu compounds, principally because the f-electrons in Pu sit at the boundary between localization and itinerancy,[1] thus presenting a challenge for modern theories of correlated electron physics.

In Pu metal interest has centered on whether or not magnetic order exists in the high temperature fcc δ phase, which occurs in pure Pu near 700 K, but can be stabilized at room temperature by alloying with a few percent Al or Ga, for example. Neutron scattering experiments[2] have set a limit of 0.04-0.4 μ$_B$ for the ordered moment in δ-Pu, but only recently have theories been able to predict such a small value.[3]

Adding to the interest in Pu-based materials, superconductivity was recently discovered[4,5] in PuCoGa$_5$ and PuRhGa$_5$. These compounds are structurally the same as their more studied Ce analogs CeCoIn$_5$ and CeIrIn$_5$ in which superconductivity is found to exist in close proximity to magnetic phases near a quantum critical point. A key question has been whether these structurally similar materials also possess similar superconducting order parameters, pairing mechanisms and associated magnetic and superconducting phase diagrams. Also relevant to the Pu superconductors is the effect of self-induced radiation damage on their intrinsic properties.

In this paper we summarize the results of muon spin relaxation (μSR) measurements carried out in α- and δ-Pu (Pu alloyed with 4.3 at. % Ga) and in the superconducting state of PuCoGa$_5$. The Pu metal studies were designed to search for evidence of magnetic ordering, and have set the most stringent limits to date for the ordered moment: $\mu_{ord} < 10^{-3}$ μ$_B$, about 40 times smaller than obtained with neutron scattering. In PuCoGa$_5$ the temperature dependence of the magnetic penetration depth λ(T) was investigated in a fresh sample and again in the same sample after 400 days of aging. We find $\lambda(T) \propto T$ for $T \leq T_c/2$, indicating a line of nodes in the superconducting order parameter. Remarkably, the temperature dependence of λ(T) is little changed even after significant radiation damage.

Our results are compared to NMR experiments[6,7] in nominally the same materials (δ-Pu, PuCoGa$_5$ and PuRhGa$_5$) to illustrate the complementarities of the techniques.

[1] J. M. Wills *et al*., J. of Electron Spectroscopy and Related Phenomena **135**, 163 (2004).

[2] J. C. Lashley *et al.* Phys. Rev. B**71**, 054416 (2005).

[3] A. B. Schick *et al.* Europhys. Lett. **69** 588 (2005); A. O. Shorikov *et al.*, Phys. Rev. B**72**, 024458 (2005).

[4] J. L. Sarrao *et al*., Nature **420**, 297 (2002).

[5] F. Wastin *et al*., J. Phys.: Condens. Matter **15**, S2279 (2003).

[6] N. J. Curro and L. Morales, MRS Society Symp. Proc. **802**, 53 (2003).

[7] Yu. Piskunov *et al*., Phys. Rev. B**71**, 174410 (2005); S. V. Verkhovskii *et al*., JETP Lett. **82**, 139 (2005).

Americium under pressure

J.-C. Griveau[*], J. Rebizant[*], R.G. Haire[§], G. Kotliar[†], G.H. Lander[*].

[*] European Commission, Joint Research Centre, Institute for Transuranium Elements Postfach 2340, 76125 Karlsruhe, Germany
[§] Oak Ridge National Laboratory (ORNL), Chemical Sciences Division, Office Box 2008, MS-6375, Oak Ridge, TN 37831, USA
[†] Center for Materials Theory, Department of Physics and Astronomy, Rutgers University, Piscataway, New Jersey 08854, USA

High-pressure measurements of the resistivity of americium metal (dhcp structure at ambient pressure) are reported to 27 GPa and down to temperatures of 0.4 K [1] under magnetic field. Americium is the first actinide element in which, at ambient pressures, the *5f* electrons may be described as localized (as in most of the *4f* rare-earth series) and thus do not participate in the bonding. Am^{3+} has an electronic ground state with a J = 0 singlet, so that (in Russell-Saunders coupling) L = –S = 3 and no magnetic moment exists. This simple picture of Am metal (6 f electrons forming an inert core decoupled from the *spd* electrons) led to the prediction [2] in 1975 of superconductivity in Am, a prediction soon verified [3] showing T_c = 0.79 K. Resistivity under pressure [4] showed that T_c rapidly increased with pressures in the GPa range. The question is when the *5f* electrons begin to affect the low-energy properties of Am. How do they affect the superconductivity when *5f* spectral weight is present at Fermi Energy, taking part in the formation of Cooper pairs? Previous studies [5] indicate that Am at ambient pressure is a type-I superconductor with a small zero-temperature critical field $H_c(0)$= 53 mT. The pressure dependence of the upper critical fields is surprising, with $H_c(0)$ increasing rapidly with pressure (~ 1 T at the maximum of T_c). The study of superconductivity in Am metal reveals that, contrary to expectations, the *5f* electrons play an important role in this material even at low pressures. Furthermore, the localization-delocalization (Mott) transition in Am is a gradual phenomenon rather than the abrupt change predicted by theory. There is no sign of any transition to ordered magnetism, as judged by an anomaly in the resistivity, in contrast to the predictions [6].

1   J.-C. Griveau, Phys. Rev. Lett. **94**, 097002 (2005)
2   B. Johansson and A. Rosengren, Phys. Rev. B **11**, 2836 (1975)
3   J. L. Smith and R. G. Haire, *Science* **200**, 535 (1978)
4   P. Link *et al*., J. Phys.: Con-dens. Matter 4, 5585 (1992).
5   J. L. Smith *et al*., J. Physique **40**, C4-138 (1979)
6   P. Söderlind *et al*., Phys. Rev. B **61**, 8119 (2000)

Many-body Electronic Structure of Americium Metal

S. Savrasov[*], K. Haule[†], G. Kotliar[†]

[*]University of California, Davis CA 95616 USA
[†]Rutgers University, Piscataway, NJ 08854 USA

INTRODUCTION

Artificially produced from Plutonium-239 in 1944, and widely used in smoke detectors Americium is the first transuranic actinide where 5f6 electrons become localized and form a closed relativistic subshell. Its recent high-pressure studies[1] have drawn much attention as understanding volume behavior in actinides systems has important consequences on their storage and disposal. They have revealed that Am undergoes a series of structural phase transitions (denoted hereafter as I, II, III, and IV) and reproduces at least two of the structures of another mysterious element, Plutonium, which links the physical behavior of all actinides materials to our fundamental understanding of bonding between their 5f- electrons. At ambient pressure Am I behaves as an ordinary metal with slightly enhanced electrical resistivity ρ(T=300K)=68 $\mu \times$ cm and no sign of ordered or disordered magnetism. This is standardly understood as a manifestation of 7F0 ground state singlet of 5f6 atomic configuration. However, the resistivity of Am raises almost an order of magnitude and reaches its value of 500 $\mu\times$cm at the orthorhombic structure of Am IV which is realized at pressures P above 16 GPa. The most prominent feature of the pressure P vs. volume V behavior is the existence of two distinct phases: the "soft" one which occurs in Am I through III as well as another "hard" phase realized in Am IV. On top of that a superconductivity in Am was first predicted[2] and then discovered[3] with Tc raising from 0.5K in Am I to 2.2K in Am II, falling slightly in Am III and then exhibiting a sharp maximum in phase IV[4].

METHOD

In this work we introduce a novel many-body electronic structure method which allows us to uncover the physics of Am. It is based on dynamical mean field theory (DMFT), a modern many body technique for treating strongly correlated electronic systems in a non-perturbative manner[5, 6] and at the same time has computational efficiency comparable with ordinary electronic structure calculations thus allowing us to deal with complicated crystal structures of real solids by self-consistent many-body calculations. Our new method considers the local Green function as a variable in the total energy functional and can be viewed as spectral density functional theory[7, 8, 9]. The advantage of such formulation as compared to original density functional theory[10] is a simultaneous access to energetics and local excitation spectra of materials with arbitrary strength of the local Coulomb interaction U.

RESULTS

The computational speed gained by our new algorithm allows us to study complicated crystal structures of Am. In particular, the existence of soft and hard phases in its equation of state can

be predicted via our self-consistent total energy calculations. Our calculation reproduces the well known fact that the f electrons in Am at zero pressure exists in a f6 7F0 configuration.

To gain theoretical insight and understand the origin of localization-delocalization transition we discuss the behavior of the electronic structure under pressure. Upon compression, the remarkable effect is observed as peak near the Fermi level gets pushed down while a resonance (small shoulder) starts forming at Ef and becomes more pronounced with increasing pressure.
The f6 ground state of the atom starts admixing an f7 configuration with a very large total spin of J=7/2. Due to hybridization with the spd bands, this large spin gets screened thus lowering the energy of the system. This is the famous Kondo mechanism, and the energy gain increases as the hybridization increases by applying pressure.

We also estimate the superconducting critical temperature by computing from first principles [11] the electron-phonon coupling of the electrons in the presence of correlations. For this purpose we have extended a newly developed dynamical mean field based linear response method, which has previously proven to provide accurate phonon spectra in correlated systems [12,13]. We estimate the coupling constant which comes out to be sufficiently high (~0.5) to predict superconductivity of the order of 1 K. The occurrence of the first maximum in experimental Tc vs pressure dependence, can then be understood as the result of the variation of the spd density of states which first increases as a result of a band structure effect but then eventually decreases as the hybridization with the f electron grows with the increase of mixed valence.

The content of this work is currently in press [14].

1   S. Heathman, R. G. Haire, T. Le Bihan, A. Lindbaum, K. Litfin, Y. Méresse, and H. Libotte, Phys. Rev. Lett. 85, 2961 (2000).
2   B. Johansson and A. Rosengren, Phys. Rev. B 11, 2836 (1975).
3   J.L. Smith and R.G. Haire, Science 200, 535(1978).
4   J.-C. Griveau, J. Rebizant, and G. H. Lander, G. Kotliar, Phys. Rev. Lett. 94, 097002 (2005).
5   Gabriel Kotliar and Dieter Vollhardt, Physics Today 57, 53 (2004).
6   A.Georges, G. Kotliar, W. Krauth and M. J. Rozenberg, Rev. Mod. Phys. 68, 13 (1996).
7   R. Chitra, and G. Kotliar, Phys. Rev. B 63, 115110 (2001).
8   S. Savrasov, G. Kotliar, and E. Abrahams, Nature 410, 793 (2001).
9   S. Y. Savrasov, G. Kotliar, Phys. Rev. B 69, 245101 (2004).
10   For a review, see, e.g., Theory of the Inhomogeneous Electron Gas, edited by S. Lundqvist and S. H. March (Plenum, New York, 1983).
11   S. Y. Savrasov, D. Y. Savrasov and O. K. Andersen, Phys. Rev. Lett. 72, 372 (1994).
12   X. Dai, S. Y. Savrasov, G. Kotliar, A. Migliori, H. Ledbetter, E. Abrahams, Science 300, 953 (2003).
13   S. Y. Savrasov, G. Kotliar, Phys. Rev. Lett. 90, 056401 (2003).
14   S. Y. Savrasov, K. Haule, G. Kotliar, Phys. Rev. Lett., in press (2006); cond-mat/0507552.

Conditions for Magnetism in Pu systems

L. Havela[*], P. Javorsky[*], F. Wastin[†], E. Colineau[†], T. Gouder[†], A.B. Shick[††], V. Drchal[††]

[*]Charles University, Faculty of Mathematics and Physics, department of Electronic Structures, Ke Karlovu 5, 121 16 Prague 2, The Czech Republic
[†]European Commission, Joint Research Centre, Institute for Transuranium Elements, Postfach 2340, 76 125 Karlsruhe, Germany
[††]Institute of Physics, Academy of Sciences of the Czech Republic, Na Slovance 2, 182 21 Prague 8, The Czech Republic

ELECTRONIC STRUCTURE OF δ-Pu

While light actinide elements are Pauli paramagnets with the itinerant $5f$ states at the Fermi level, the localization for actinides behind Am leads to magnetic ordering analogous to lanthanides. The specific position of Pu just before the localization threshold should make it very sensitive to external variables, but various Pu allotropic phases have surprisingly nearly identical weak magnetic susceptibility, despite a large volume expansion exceeding 20% for the *fcc* δ-Pu comparing to monoclinic α-Pu. This situation poses a problem for theoretical description, because LDA or GGA calculations indicate the formation of magnetic moments for the expanded phases[1]. Our recent LDA+U calculations[2] (*around mean field* version), which yield a non-magnetic ground state ($S = 0. L = 0$) and correct cohesion properties, suggest that the key, at least for δ–Pu, can be the $5f$-count approaching the non-magnetic $5f^6$ state, i.e. much higher than the originally expected value close to 5.0. The calculations also indicate[3] that the magnetic order is not established, when the lattice is expanded by Am doping, or if the dimensionality is reduced. For the terminal concentration of pure Am the LDA+U calculations[3] correctly reproduce the non-magnetic $5f^6$ state.

The main characteristics of the Pu-$5f$ states is the density of one–electron states concentrated around 1 eV binding energy, while the empty states of the $5f_{7/2}$ character are about 4 eV above E_F. Variations with increasing Am concentration in the *fcc* Pu-Am solid solution were found negligible. If this picture is credible, the high value of the *g*-coefficient of low-temperature electronic specific heat, as well as high-intensity *f*-emission observed close to E_F by PES, should have been due to many-body states, as suggested in Refs.4,5. One way to test the adequacy of our LDA+U calculations is to study experimentally the behaviour of expanded Pu. For this purpose, the doping by Am is the most efficient tool. Unlike the common δ-phase stabilizing dopings by Al or Ga, the doping by Am expands the lattice, and the expansion is larger than e.g. for the Ce doping.

Considering the alternative scenario, at which a narrow $5f$ band at E_F is the key ingredient bringing δ-Pu to the verge of magnetism, such expansion should lead to increase of *g*, presumably to onset on magnetic order, and all properties would undergo a dramatic development due to the changing density of one-electron states at E_F, increasing up until it is suddenly forced to leave the Fermi level due to incipient localization.

PROPERTIES OF Pu-Am SYSTEM

Am doping to Pu corresponds to a dilution by a non-magnetic element. Magnetic susceptibility of Am is rather high (the value approaching $1*10^{-8}$ m^3/mol [6]) due to the Van Vleck susceptibility of the $5f^6$ state with $J = 0$. The behaviour of Am under pressure[7,8] suggests that the localized character is not affected even if the volume is compressed to the volume of δ-Pu. We can therefore assume that the non-magnetic character of Am stays throughout the Pu-Am system at ambient pressure. This is corroborated by rather invariable character of Am electronic states obtained from calculations mentioned above. In fact, Pu and Am are not completely miscible, but the *fcc* structure extends at least to 75% Am, while remaining as a high-temperature phase of pure Am. Here we review recent results on Pu-Am system using photoelectron spectroscopy (PES) and specific heat. Although PES does not bring any direct information on a possible magnetic order, the invariable character of the Pu-$5f$ states, evidenced for concentration to about 30% Am, excludes any noticeable change of the ground state. Moreover, the *g*-values weakly decrease with increasing Am concentration, even if they are normalized per mole of Pu (assuming a negligible contribution from Am, as $g_{Am} = 2$ mJ/mol K^2), from 60 mJ/mol Pu K^2 for Pu-8%Am to 48 mJ/mol Pu K^2

for Pu-15% Am. These findings, together with the observed insensitivity of electrical resistivity and magnetic susceptibility[9] to the volume expansion (3.5% for Pu-20% Am comparing to pure δ-Pu), indicate that the alternative $5f$ narrow-band scenario is not tenable for δ-Pu.

WHICH Pu SYSTEMS CAN BE MAGNETIC?

The non-magnetic character of δ-Pu is well established[10,11]. We have been showing that the important feature of the non-magnetic ground state could be the proximity of the $5f$ count obtained to the non-magnetic $5f^6$ singlet. The LDA+U calculations indicate that even if such state is hybridized with conduction electrons and part of the $5f$ charge is lost, the hole in the $5f_{5/2}$ states can remain isotropic, i.e. without any spin or orbital polarization. Such state can be then robust with respect to lattice expansion or reducing the dimensionality. A hint how to reach a magnetic state for Pu would be to allow for a higher depletion of the $5f$ states by hybridization in a compound, while keeping the $5f$ band narrow enough in the sense of Hill limit arguments. Inspecting the occurrence of Pu magnetism, we can understand why the Pu chalcogenides PuS, PuSe, PuTe are weakly magnetic, while the pnictides as PuSb, with one less electron and assumed $5f^5$ state, are magnetically ordered[12]. Another instructive example is the behaviour of Pu in diluted alloys. For example, Pu has magnetic moment as diluted in Pd,[13] which contrasts with non-magnetic U diluted in Pd.[13] A certain charge transfer towards the Pd-4d states, induced by the large difference in electronegativity of Pd and the actinides, which probably eliminates the U moments, can give rise to the Pu moments. As a conclusion, we suggest that a reduction of the $5f$ count due to bonding is a necessary pre-requisite for Pu magnetism, which is indeed observed in many compounds.

1   P. Söderlind, A. Landa, B. Sadigh, Phys.Rev.B **66**, 205 109 (2002).
2   A.B. Shick, V. Drchal, L. Havela, Europhys.Lett. **69**, 588 (2005).
3   A.B. Shick, L. Havela, J. Kolorenc, V. Drchal, T. Gouder, P.M. Oppeneer, Phys.Rev.B, in press.
4   S.Y. Savrasov, G. Kotliar, E. Abrahams, Nature **410**, 793 (2001).
5   L.V. Pourovskii, M.I. Katsnelson, A.I. Lichtenstein, L. Havela, T. Gouder, F. Wastin, A.B. Shick, V. Drchal, G.H. Lander, Europhys. Lett., in press
6   B. Kanellakopulos, A. Blaise, J.M. Fournier, Solid State Commun. **17**, 713 (1975).
7   A. Lindbaum, S. Heathman, K. Litfin, Y. Meresse, R.G. Haire, T. Le Bihan, H. Libotte, Phys.Rev.B **63**, 214101 (2001).
8   J.-C. Griveau, J. Rebizant, G.H. Lander, G. Kotliar, Phys.Rev.Lett. **94**, 097002 (2005).
9   N. Baclet et al., to be published.
10   J.C. Lashley, A. Lawson, R.J.McQueeney, G.H. Lander, Phys.Rev.B **72**, 054416 (2005).
11   R.H. Heffner et al., arXiv:cond-mat/0508694, (2005)
12   see various chapters in Handbook on the Physics and Chemistry of the Actinides, edited by A.J. Freeman and G.H. Lander, vols. 1 and 2, North Holland , Amsterdam, 1985
13   W.J. Nellis and M.B. Brodsky, Phys.Rev.B **4**, 1594 (1971).

Subsurface Bio-mediated Reduction of Higher-Valent Uranium and Plutonium

D. T. Reed[*], G. Smith[#], R. Deo[+], B. Rittmann[+], J. F. Lucchini[*],
M. Borkowski[*], M. K. Richmann[*]

[*] Earth and Environmental Sciences Division, Los Alamos National Laboratory, Carlsbad NM
  88220 USA
[#] Department of Biology, New Mexico State University, Las Cruces NM 88003 USA
[+] Center for Environmental Biotechnology, Arizona State University, Tempe AZ 85282 USA

INTRODUCTION

The role and importance of redox reactions in determining actinide subsurface mobility are beyond question. In the subsurface, redox control is often established by the iron mineralogy and associated aqueous chemistry[1, 2]. There is also a growing recognition of the important role microbiological processes have in defining the redox chemistry of multivalent actinide species[3, 4] by both direct and indirect means. The mechanisms by which redox control is established is a key aspect of remediation and immobilization strategies for actinides when they are present as subsurface contaminants.

The important effects of redox-active minerals (e.g. iron and iron oxides) and microbial processes on subsurface redox processes are not mutually exclusive[5]. Metal reducing bacteria often modulate the oxidation state of aqueous iron species and can solubilize iron to increase its bioavailability. It is this coupling of biological and geochemical processes, and correspondingly its effect on actinide speciation, that is the focus of our current studies. Progress made in the study of bio-mediated reduction pathways towards the reduction of Pu (VI) and U (VI) species by *S. algae BrY* under anoxic conditions is reported.

EXPERIMENTAL APPROACH

Shewanella Algae strain *BrY* is a dissimilatory gram negative iron reducing bacteria that was isolated from the Great Bay estuary, New Hampshire[6]. It is a facultative anaerobe that was grown aerobically on tryptic soy broth prior to use. Cells were harvested, rinsed in PIPES media, concentrated by centrifugation, and then re-suspended to prepare an inoculum stock prior to addition into the various growth media in an anoxic glovebox, where the experiments were conducted.

Uranium (as UO_2^{2+}) and plutonium (as PuO_2^{2+} or PuO_2^+) were the initial species added to the various growth media or groundwater simulants (~pH 7-8). Iron, when present, was added as a stabilized Fe^{3+} - NTA complex. Lactate was used as the electron donor. Total uranium, iron, and plutonium concentrations were determined by ICP-MS (Agilent) specially configured for iron analysis. Lactate was analyzed using a lactate analysis kit based on a colorimetric technique. NTA and other organics were analyzed by ion chromatography (Dionex DX 500). Absorption spectrometry (CARY 500) was used to establish and confirm the actinide and iron oxidation states.

RESULTS AND DISCUSSION

Abiotic and biotic experiments were performed. In the abiotic experiments, Pu(VI) and U(VI) were added to pH ~ 7-8 groundwater in the presence of iron and iron oxides to establish the redox trends. Example results for Pu(VI) and iron oxides are shown in Figure 1. Here it was observed that on a timeframe of less than 100 hours almost all the Pu(VI) was reduced when reduced iron was present. The most rapid reduction rate was observed with magnetite and attributed to the presence of Fe(II) in the oxide. The corresponding decrease in total plutonium concentration to sub-micromolar concentrations is indicative of a redox process where Pu(IV/III) species are being generated. When only Fe(III) was present, as was the case with hematite, the plutonium concentration did not decrease substantially but essentially all the Pu(VI) was reduced to Pu(V). U (VI), under similar conditions, was stable towards reduction for over a year although eventually reduction was noted.

Figure 1. Reduction of Pu(VI) by Iron and Iron Oxides
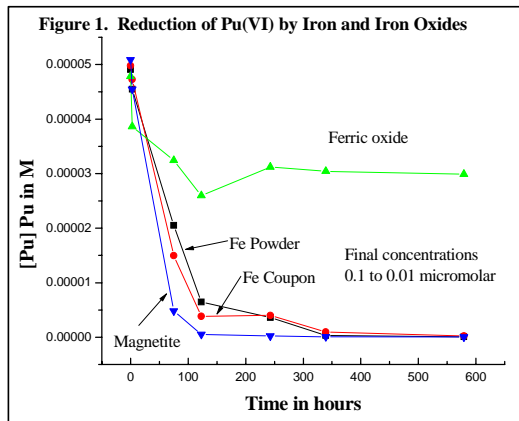
In the biotic experiments performed, the goal was to establish the conditions and key mechanisms leading to actinide reduction. Direct and indirect (co-metabolic) pathways for reduction exist. In the presence of *S. algae*, and 10 mM of Fe^{3+} as an NTA complex, no reduction of iron or uranium was noted under aerobic conditions. When anaerobic conditions were established both iron (III) and uranium (VI) were reduced (see Figure 2). Although uranium precipitated, iron remained solubilized as an Fe^{2+} complex. Analogous results were obtained with plutonium but there is a much greater effect of abiotic processes and reactions. Establishing the mechanistic details of these abiotic and direct/indirect biotic processes is the subject of ongoing research.
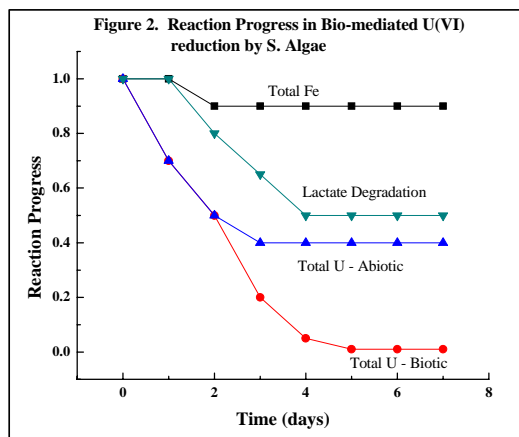
Figure 2. Reaction Progress in Bio-mediated U(VI) reduction by S. Algae

1. D.T. Reed, J.F. Lucchini, S.B. Aase, and A.J. Kropf, accepted in Radiochim Acta, (2006)
2. J. Farrell, W.D. Bostick, R.J. Jarabeck, and J.N. Fiedor, Ground Water 37(4), 618 (1999).
3. J.E. Banaszak, B.E. Rittmann, and D.T. Reed, J. Radioanal. Nuc. Ch. 241, 385 (1999).
4. B.E. Rittmann, J.E. Banaszak, and D.T. Reed, Biodegradation, 13(5) 329-42 (2002).
5. D. Fortin and S. Langley, Earth-Sciences Reviews 72, 1-19 (2005).
6. F. Caccavo, R.P. Blakemore, D.R. Lovley, Appl. Environ. Microbiol. 58, 3211-3216 (1992).

Disproportionation of Pu(IV) or a two step mechanism?
Redox behavior of Pu(IV) in acidic solutions

C. Walther*, H.R. Cho*, C.M. Marquardt*, V. Neck*, A. Seibert[†], J.I. Yun* and Th. Fanghänel*[,‡]

*Forschungszentrum Karlsruhe, Institut für Nukleare Entsorgung, D-76021 Karlsruhe, Germany
[†]European Commission, JRC, Inst. For Transuranium Elements, D-76125 Karlsruhe, Germany
[‡] Physikalisch-Chemisches Institut, Ruprecht-Karls Universität,
   Im Neuenheimer Feld 253, D-69120 Heidelberg, Germany

The redox behavior of plutonium in acidic solutions has been studied for many decades. The formation of Pu(III), Pu(V) and Pu(VI) in Pu(IV) solutions exposed to air is usually ascribed to the disproportionation of Pu(IV) into Pu(III) and Pu(V), followed by the reaction of Pu(V) with Pu(IV) or the disproportionation of Pu(V) into Pu(III) and Pu(VI).[1-4] As the measured oxidation state distributions led to doubts on this reaction path,[3,5] we have revisited this topic and studied 10^{-5} to $5 \cdot 10^{-4}$ M Pu(IV) solutions (pH_c = 0.3 - 2.1 in 0.5 M HCl/NaCl, 22°C) as a function of time. The solutions were obtained by dilution of electrochemically prepared Pu(IV) stock solutions. The concentrations of $Pu^{IV}(aq)$, Pu^{3+}, PuO_2^+ and PuO_2^{2+} were determined by UV/Vis/NIR absorption spectroscopy, using a 1m-capillary cell for low concentrations. Partly the solutions were colloid-free, partly they included Pu(IV) colloids, in particular at Pu(IV) and H^+ concentrations above the reported solubility of $PuO_2(am, hyd)$.[6] The presence or absence of Pu(IV) oxyhydroxide colloids > 5 nm was confirmed by laser-induced breakdown detection (LIBD)[5,6] . As the fraction of polymeric or colloidal Pu(IV) cannot be quantified by spectroscopy it was calculated from the difference $[Pu]_{tot} - \{[Pu^{IV}_{aq}] + [Pu^{3+}] + [PuO_2^+] + [PuO_2^{2+}]\}$.

The disproportionation of Pu(IV) solutions at pH 0 - 2 leads to Pu(III) and, depending on pH, to Pu(V), Pu(VI) or both[1-4] : $3\ Pu^{4+} + 2\ H_2O \Leftrightarrow 2\ Pu^{3+} + PuO_2^{2+} + 4\ H^+$
Accordingly and independent of whether an equilibrium state is reached or not, the following balance must be valid for Pu(III), Pu(V) and Pu(VI) formed from Pu(IV):[3]

$$[Pu(III)] = [Pu(V)] + 2\ [Pu(VI)] \tag{1}$$

However, none of the solutions investigated in the present study (two examples are shown in Fig.1) fulfils this balance at reaction times < 10 days. Instead, the formation of Pu(III) is always approximately equal to the simultaneous decrease of Pu(IV)aq (Fig.1, left):

$$d[Pu(III))/dt = - d[Pu(IV)_{aq}]/dt \tag{2}$$

i.e., $\{[Pu(IV)aq] + [Pu(III)]\}$ = constant and, as a consequence:

$$d\{[Pu(V)] + [Pu(VI)]\}/dt = - d[Pu(IV)_{coll}]/dt. \tag{3}$$

At concentrations above the solubility of $PuO_2(am, hyd)$ (Fig.1, right) it is directly observed, that $[Pu(IV)_{coll}] + [Pu(V)]$ remains constant.
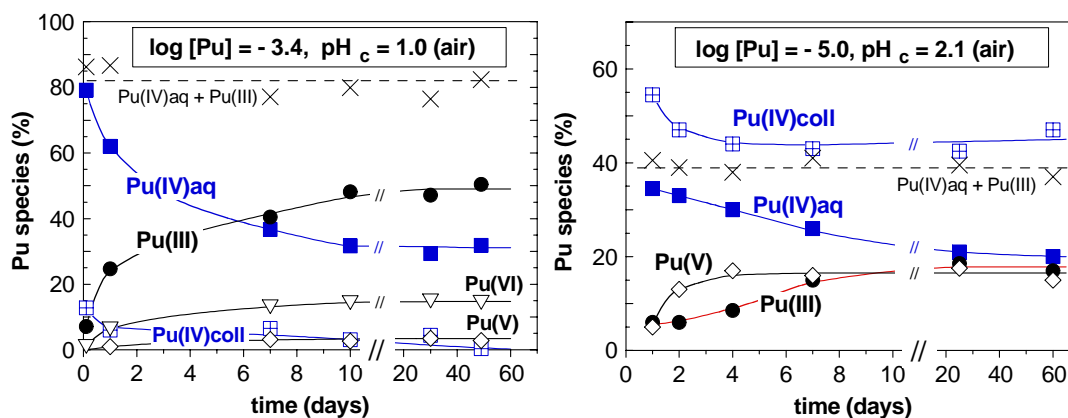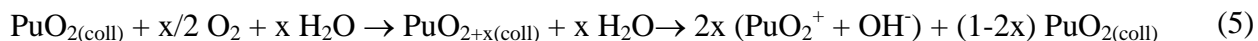
Fig 1: Oxidation state distributions of initially Pu(IV) solutions as a function of time
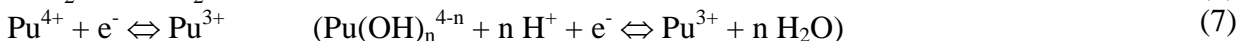
The present results indicate that the so-called 'disproportionation of Pu(IV)' is a two-step process. The initial step is the formation of PuO_2^+, either by the redox equilibrium with $PuO_{2(am, hyd)}$[7,8] which is equal to $PuO_n(OH)_{4-2n} \cdot xH_2O$ colloids > 5 nm:

$$PuO_{2(coll, hyd)} \Leftrightarrow PuO_2^+ + e^- \tag{4}$$

or by the oxidation of colloidal or smaller polynuclear Pu(IV) species by O_2, analogous to the water-catalyzed oxidation of solid $PuO_{2(s, hyd)}$ to $PuO_{2+x(s, hyd)}$,[9] followed by the dissolution of the oxidized Pu(V) fractions:

$$PuO_{2(coll)} + x/2\ O_2 + x\ H_2O \rightarrow PuO_{2+x(coll)} + x\ H_2O \rightarrow 2x\ (PuO_2^+ + OH^-) + (1-2x)\ PuO_{2(coll)} \tag{5}$$

The second step is the simultaneous equilibration of the redox couples Pu(V)/Pu(VI) and Pu(IV)/Pu(III) which are related by pe (and pH because of Pu(IV) hydrolysis equilibria):

$$PuO_2^+ \Leftrightarrow PuO_2^{2+} + e^- \tag{6}$$
$$Pu^{4+} + e^- \Leftrightarrow Pu^{3+} \qquad (Pu(OH)_n^{4-n} + n\ H^+ + e^- \Leftrightarrow Pu^{3+} + n\ H_2O) \tag{7}$$

This mechanism explains that the sum $\{[Pu(III)] + [Pu(IV)_{aq}]\}$ always remains constant. It also explains that colloid-free Pu(IV) solutions at very low pH (e.g. pH 0.3), *i.e.*, far below the solubility of $PuO_2(am, hyd)$,[6] reacts much more slowly and to a lesser extent than at pH = 1.0 where polynuclear and colloidal Pu(IV) is formed immediately. In the experiment at $[Pu]_{tot} = 1.0 \cdot 10^{-5}$ M and $pH_c = 2.1$ (Fig. 1,right), considerably above the solubility of $PuO_2(am, hyd)$,[6] Pu(V) is evidently formed faster than Pu(III), not simultaneously as required by the disproportionation reaction.

The oxidation state distributions and pe values measured after equilibration times of more than 20 days are consistent with the known redox equilibria (4), (6) and (7).[7,8,10] The 'disproportionation' reactions also describe correctly equilibrium state thermodynamics, but not the underlying reaction mechanism.

1   R.E. Connick and W.H. McVey, J. Am. Chem. Soc., **75**, 474,(1953)
2   S.W. Rabideau, J. Am. Chem. Soc., **75**, 798 (1953) and **79**, 6350 (1957)
3   D.A. Costanzo, R.E. Biggers and J.T. Bell, J. Inorg. Nucl. Chem., **35**, 609 (1973)
4   H. Capdevila, P. Vitorge and E. Giffaut, Radiochim. Acta, **58/59**, 45 (1992)
5   C. Walther, C. Bitea, J.I. Yun, J.I. Kim, Th. Fanghänel, C.M. Marquardt, V. Neck and A. Seibert, Actinides Research Quarterly, Los Alamos Natl. Lab., **11**, 12 (2003)
6   R. Knopp, V. Neck and J.I. Kim, Radiochim. Acta, **86**, 101 (1999)
7   D. Rai, Radiochim. Acta, **35**, 97 (1984)
8   H. Capdevila and P. Vitorge, Radiochim. Acta, **82**, 11 (1998)
9   J.M. Haschke and V.M. Oversby, J. Nucl. Mat., **305**, 187 (2002)
10 R.J. Lemire, J. Fuger, H. Nitsche, P. Potter, M.H. Rand, J. Rydberg, K. Spahiu, J.C. Sullivan, W.J. Ullman, P. Vitorge, H. Wanner (OECD,NEA-TDB). *Chem. Thermodyn. Neptunium & Plutonium.* Elsevier, Holland, (2001)

Plutonium Speciation in Environmental Systems, From Hydrolysis to Aerobic and Anaerobic Biogeochemistry

M. P. Neu[*], S. D. Reilly[*], W. Runde, S. A. Stout[*] and H. Boukhalfa[*]

[*]Los Alamos National Laboratory, Los Alamos CA 87545 USA

Plutonium is present in the environment as a result of nuclear energy and weapons production. Surfacial contamination can be removed Given the impressive sensitivity of radioanalytical methods and mass spectroscopy, the transport of residual contamination can be detected and tracked . However the form of Pu can rarely be determined from direct characterization. Generally, the concentration of plutonium is too low or the conditions of the measurement(s) are different from the conditions at the sample site. Thus, the plutonium migration can be observed, but not predicted since the mechanism of transport can not be discerned.

In order to develop an ability to forecast the stability and long-term fate of plutonium we must understand fundamental plutonium redox, complexation reactions, surface reactions, and coupled biogeochemical processes that can be individually parameterized and systematically combined. Together with site-specific properties, such as the chemical composition and Eh of the water, the microscopic and macroscopic mineralogy, the amount and viability of microorganisms present, and the underlying hydrology and geomorphology of the region, these thermodynamic and kinetic values can be used in fate and transport codes. This presentation will review the mechanisms and reactions that have been reported and the research that remains to realize a predictive model of plutonium speciation and resultant mobility in aqueous environmental systems.

U(VI) Silicate Solid Phases as Sinks for Sequestration of Non-U f-element Cations in the Environment

S. B. Clark[*]

[*]Washington State University, Department of Chemistry, Pullman, WA, 99164-4630

INTRODUCTION

If used nuclear fuel is disposed of in a high-level waste repository without reprocessing, the uranium fuel will oxidize on a geologic time scale to form U(VI) solids. The 1:1 uranyl silicate minerals such as uranophane ($Ca[(UO_2)_2(SiO_3OH)_2]\cdot5(H_2O)$) and boltwoodite ((Na, K)$[(UO_2)(SiO_3OH)](H_2O)_{1.5}$) may be important solids for controlling the environmental availability of other f-elements that are produced during neutron irradiation. These solids provide surfaces to which the non-U f-elements may sorb or solids into which they may be incorporated. Often, very finely divided nano-materials are present, and appear to play an important role in sequestration. Defining mechanisms of sorption and/or incorporation of these f-elements along with thermodynamic descriptions of these processes are needed for performance assessment activities in high level waste disposal. In this presentation, the chemistry of these U(VI)-silicate solids will be explored, along with the partitioning of non-U f-elements to them.

EUROPIUM PARTITIONING INTO URANOPHANE[1]

Uranophane was synthesized with various mole ratios of $Eu^{3+}:Ca^{2+}$ present. In all solids prepared, the Eu^{3+} was sequestered to the U(VI) silicate solid formed. Powder x-ray diffractograms of the resulting solids indicated that on the bulk-level, the uranophane structure was preserved when the mole ratio of $Eu^{3+}:Ca^{2+}$ remained below 10%. At higher levels of Eu^{3+}, a crystalline solid was formed that was not consistent with the uranophane structure. For those solids with 10% or less Eu^{3+} present, transmission electron microscopy analysis of the solid indicates that the bulk material is actually a mixture of needle-like materials as expected for uranophane, and additional finely divided materials with diffraction patterns that are not consistent with uranophane. Microscale elemental analysis of these materials indicates that the polycrystalline solids are largely responsible for sequestration of most of the Eu^{3+}. The uranophane needles do incorporate small quantities of Eu^{3+}, but never more than 5 mole %.

NEPTUNIUM PARTITIONING TO URANOPHANE[2]

In this case, both uranophane and sodium boltwoodite were prepared in the presence of trace quantities of neptunium (V) as the NpO_2^+ cation (0.5 – 2.0 mole %, relative to U). In all cases, the Np is quantitatively sequestered into the U(VI) silicate solid. The presence of the Np did not alter the powder diffraction patterns of the resulting solids. Individual crystallites of the solids were analyzed with transmission electron microscopy and electron energy loss

spectroscopy to demonstrate that Np is associated with isolated solids. No evidence for discrete Np phases such as Np oxides was observed.

SUMMARY

These results will be described for Eu^{3+} and NpO_2^+ partitioning into the 1:1 U(VI) silicate solids. The structures of uranophane and boltwoodite will be described along with the possibilities for Eu^{3+} and NpO_2^+ substitution into the solids. Where possible, incorporation will be distinguished from sorption. In both cases, thermodynamic approaches for treating these processes during modelling will be described.

1   Matthew Douglas, Washington State University PhD Thesis; "Uranium(VI) solid phases formed in the presence of Np and other metal cations", 2005.
2   M. Douglas, S. B. Clark, J. I. Friese, B. W. Arey, E. C. Buck, B. D. Hanson, S. Utsunomiya, and R. C. Ewing, "Microscale characterization of U(VI) silicate solids and associated Np", *Radiochimica Acta*, **93**, 265-272 (2005).

Radionuclide Distribution in Debris from Underground Nuclear Tests Detonated in Silicate and Carbonate Rocks

M. Zavarin, P. Zhao, Q. Hu, T. P. Rose, and A. B. Kersting

Chemical Biology and Nuclear Science Division, Lawrence Livermore National Laboratory, Livermore, CA, USA 94551

Underground nuclear detonations produce a diverse suite of radionuclides that includes tritium, fission products, activation products, and residual actinide fuel[1]. The initial distribution of these species within a test cavity and chimney is determined by the temperature and pressure history immediately following the explosion.[2] Refractory species that condense at high temperatures tend to be partitioned into the 'melt glass', while volatile species that condense at lower temperatures tend to be more widely dispersed throughout the rubblized cavity-chimney environment. Recommendations for radionuclide partitioning have been published[3], but for many species there is still a significant margin of uncertainty in these estimates. Furthermore, radionuclide partitioning has been developed only for tests conducted in rock or alluvium dominated by aluminosilicate minerals. No such partitioning information is available for tests conducted in carbonate rock (Figure 1).
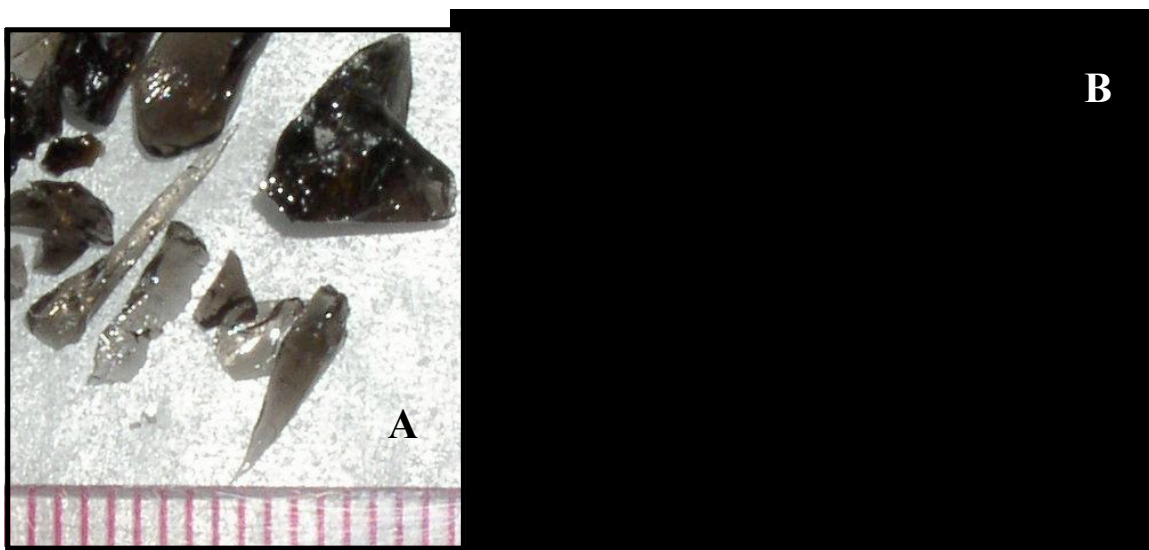

Fig 1: Photographs illustrating the textural characteristics of nuclear test debris. (A) Dark-colored aluminosilicate melt glass exhibiting typical 'obsidian-like' textures and (B) Friable, chalk-like carbonate test debris exhibiting only minor glassy and iron-oxide stained fragments.

We will describe the results of two separate investigations into the physical and chemical distribution of radionuclides in underground nuclear test cavities at the Nevada Test Site (NTS). In 2005, we investigated radionuclide redistribution from the Chancellor test. The Chancellor test was detonated in the U-19ad emplacement hole on 1 September 1983 at a vertical depth of 2,047 ft (624 m) below the surface of Pahute Mesa, NTS. It has an announced yield of 143 kt.[4]

The test was conducted in the Tertiary rhyolite of Echo Peak[5], a devitrified lava of the Paintbrush Group that erupted from the Claim Canyon Caldera approximately 12.8 million years ago[6]. For plutonium, 1.5% of the inventory is contained in the rubble fraction and 98.5% is present in the melt glass. These results are in agreement with estimates reported by the IAEA[3] (2% rubble, 98% glass). However, they differ from the 0% rubble fractionation (100% in glass) reported by the French[3] and are less conservative than the 5% rubble fractionation (95% in glass) used in recent radionuclide contaminant transport models at the NTS. For uranium, approximately 94% of the test-derived uranium is contained in the melt glass, and 6% is in the rubble. The uranium fraction in the rubble is somewhat lower than the IAEA estimate of 10%. However, compared to plutonium, it is apparent that uranium is more volatile and is redistributed more widely in the nuclear test cavity.

Presently, we are investigating the radionuclide distribution in tests conducted in carbonate rock. Only four tests were conducted in the carbonate rock in Yucca Flat, NTS. However, two tests are located close enough to saturated water table to provide a direct path for radiologic contamination of the regional carbonate aquifer. We expect the partitioning of Pu and U in the debris from carbonate tests to differ significantly from that of tests conducted in aluminosilicate rock due to their widely differing early time pressure, temperature, and rock condensation histories. We will describe the partitioning of various classes of radionuclides between the "melt glass" and rubble in carbonate tests and compare these results to the partitioning behaviour observed in the Chancellor test. Furthermore, we will describe how the Underground Test Area (UGTA) project utilizes this partitioning information to develop radionuclide reactive transport models and predict the extent of groundwater contamination at the NTS.

1   S.M. Bowen, *et al.,* Nevada Test Site Radionuclide Inventory, 1951-1992. Los Alamos National Laboratory, LA-13859-MS (2001).
2   I.Y. Borg, R. Stone, H.B. Levy, and L.D. Ramspott, Information Pertinent to the Migration of Radionuclides in Ground Water at the Nevada Test Site. Part 1: Review and Analysis of Existing Information. Lawrence Livermore National Laboratory, UCRL-52078 Pt. 1 (1976).
3   IAEA, The Radiological Situation at the Atolls of Mururoa and Fangataufa, Technical Report, Volume 3: Inventory of Radionuclides Underground at the Atolls. International Atomic Energy Agency, Vienna, Austria, IAEA-MFTR-3 (1998).
4   DOE/NV, United States Nuclear Tests, July 1945 through September 1992. U.S. Department of Energy, Nevada Operations Office, Las Vegas. DOE/NV-209 (Rev. 15) (2000).
5   Pawloski, G.A., *et al.,* Categorization of Underground Nuclear Tests on Pahute Mesa, Nevada Test Site, for Use in Radionuclide Transport Models. Lawrence Livermore National Laboratory, UCRL-TR-208347 (2002).
6   Sawyer, D.A., *et al.,* Episodic caldera volcanism in the Miocene southwestern Nevada volcanic field: revised stratigraphic framework, $^{40}Ar/^{39}Ar$ geochronology, and implications for magmatism and extension. Geol. Soc. Am. Bull., **106**: 1304 (1994).

Microbial Transformations of Plutonium

A. J. Francis, C.J. Dodge and J.B. Gillow
Environmental Sciences Department, Brookhaven National Laboratory, Upton, NY 11973, USA

The presence of Pu in transuranic (TRU)- and mixed-wastes together with organic compounds, is a major concern because of the potential for migration from the waste repositories and contamination of the environment[1-4]. Pu exists in several oxidation states (III, IV, V, VI) and as various chemical species (salts, organic complexes, colloids) having a very complex chemistry and environmental behavior. Soil pH, the presence of organics, redox conditions, mineralogy, and microbial activity affect the chemical speciation of Pu[1-5]. Chelating agents, such as citric acid, are present in Waste Isolation Pilot Plant (WIPP) TRU and mixed wastes. Citric acid forms a strong complex with Pu(IV) and has been used in extracting [239]Pu from contaminated soil.

Microorganisms have been detected in low-level radioactive wastes, TRU wastes, Pu-contaminated soils, and in current and planned waste-repository sites for disposal of nuclear waste. Leachates collected from the low-level radioactive-waste sites contained [238, 239, 240]Pu (gross alpha activity of 1.7×10^5 pCi/L), aerobic- and anaerobic- bacteria (*Bacillus* sp., *Pseudomonas* sp., *Citrobacter* sp., and *Clostridium* sp.) and organic compounds[1,2,4]. The radioactive- and organic-chemicals in the leachate were not toxic to the bacteria. Metabolically active microbes were identified at the LANL's TRU waste burial site containing [239]Pu-contaminated soil. Microorganisms present in the radioactive wastes can affect the long-term stability of radionuclides. We investigated the biotransformation of Pu-citrate and Pu-nitrate by aerobic and anaerobic bacteria, respectively.

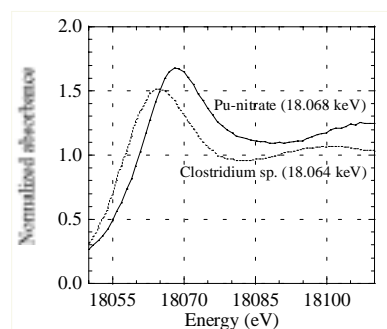**Reductive dissolution of Pu(IV) by the anaerobic bacterium *Clostridium* sp.** Addition of 1×10^{-7} M [242]Pu (IV)-nitrate had no effect upon the growth and metabolism of glucose of *Clostridium* sp. Plutonium added to the bacterial growth medium (uninoculated control) resulted in its precipitation and was removed by 0.4µm filtration. Speciation calculations showed that Pu most likely existed as $Pu(OH)_4$ at pH 6.2 due to hydrolysis and polymerization. The growth of the bacterium lowered the Eh of the medium from +50 mV to -180 mV), and the pH from 6.2 to 2.8, concomitant with the production of acetic and butyric, acids and carbon dioxide (225 µmol). After 14h of growth, 70% of the Pu passed through a 0.4 µm filter and 55% passed through a 0.03 µm filter suggesting a significant portion of Pu was solubilized. Solvent extraction by thenoyltrifluoroacetone (TTA) confirmed a decrease in the polymeric form of Pu and an increase in the soluble fraction, suggesting the presence of Pu^{3+}. XANES analysis of the culture at the Pu L_{III} edge (18.057 keV) confirmed that the oxidation state was Pu^{3+} (Figure 1). The Eh of the medium was low and the CO_2 concentration high, thus favouring the reduction of Pu from the tetravalent to the trivalent state. These results suggest that under appropriate conditions Pu can be reduced to Pu(III) by anaerobic bacteria.

Fig 1. XANES analyses of Pu before and after bacterial action.

Biotransformation of Pu(IV)-citrate complex by *Pseudomonas fluorescens*. Electrospray ionization-mass spectrometry (ESI-MS) analysis of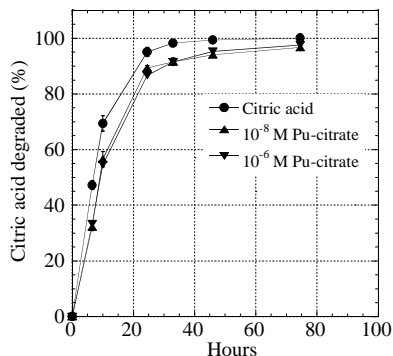 ^{242}Pu-citrate in the presence of excess citric acid indicated the presence of a biligand Pu-cit$_2$ complex. XANES and EXAFS analyses showed that Pu was in the +4 oxidation state and associated with citric acid as a mononuclear complex. The metabolism of citric acid by *P. fluorescens* was not affected by the presence of 10^{-5} M Pu. The Pu-citrate complex is relatively stable in the absence of bacterial activity. However, in the presence of bacteria and after complete metabolism of citrate, solvent extraction by TTA and microfiltration (0.03 µm) of the medium showed that the Pu was present in the polymeric form. High ionic strength (0.9M) of the medium affected citrate metabolism, and Pu remained in solution complexed with citric acid. The extent of formation of the Pu polymer depended on the Pu:citrate ratio, the extent of citrate metabolism, and the ionic strength of the medium.

Fig 2. Effect of adding ^{242}Pu on citrate metabolism. Citric-acid concentration is 10^{-4} M.

Mobilization of Pu from contaminated Soils. Chemical characterization of Pu at contaminated sites shows that its environmental form varies according to the site and the waste stream. For example, at Rocky Flats, CO, the predominant form appears to be as PuO$_2$(s); at the Nevada Test Site Pu was associated with mineral colloids; while, at Oak Ridge, TN it is associated with organic matter. Pu is generally considered to be relatively immobile; however, its transport, albeit at very low concentrations, has been observed at several DOE sites including Rocky Flats (RF), Los Alamos National Laboratory (LANL), and Nevada Test Site (NTS)[6]. Plutonium in surface waters at the RF site was shown to be associated with organic macromolecules[7]. Studies with Pu contaminated soils show that Pu and other radionuclides can be remobilized due to enhanced aerobic or anaerobic microbial activity. Studies are under way to determine the mechanisms of dissolution of Pu from contaminated soils.

References
1   A.J. Francis. 1990 *Experientia* 46: 840.
2   A.J. Francis, *In Plutonium in the Environment* A. Kudo, (Ed) Elsevier Science Ltd., Co., UK. 2001, pp 201-219.
3   R. E.Wildung, and T. R. Garland. 1982. *Appl. Environ. Microbiol.43*: 418.
4   M.P. Neu, C.E. Ruggiero, and A.J. Francis. Bioinorganic Chemistry of Plutonium and Interactions of Plutonium with microorganisms and Plants. In "Advances in Plutonium Chemistry 1967-2000" D. Hoffman (Ed), 2002 pp 169-211. ANS, La Grange Park Illinois and University Research Alliance, Amarillo, Texas.
5   P.A. Rusin, L. Quintana, J.R. Brainard, B.A. Strietelmeier, C.D.Tait, S.A. Ekberg, P.D. Palmer, T.W. Newton, and D.L. Clark. 1994. *Environ. Sci. Technol*. 28: 1686.
6   A.B Kersting. D.W. Efurd, D.L. Finnegan, D.K. Rokop, D.K. Smith, and J.L. Thomson. *Nature*. 1999, 397: 56.
7   P.H Santschi, K. Roberts, and L. Guo. 2002. The organic nature of colloidal actinides transported in surface water environments. *Environ. Sci. Technol*. 36: 3711-3719.

Actinide Sorption by Well-Characterized Colloid Particles.
Redox Speciation and Surface Complexation Modelling.

S.N. Kalmykov[*], A.P. Novikov[†], A.B. Khasanova[*], Yu.A.Teterin[††], B.F. Myasoedov[†], S.B. Clark[†††]

[*]Lomonosov Moscow State University, Chemistry department, Moscow 119992, Russia

[†]Vernadsky Institute of Geochemistry and Analytical Chemistry, Moscow 119991, Russia

[††]Research Centre "Kurchatov Institute", Moscow 123182, Russia

[†††]Washington State University, Pullman WA 99164, USA

INTRODUCTION

Colloids are submicron particles ubiquitous in the subsurface environment. Due to high surface to mass ratio and small size they may be responsible for facilitated transport of contaminants including actinides. For facilitated transport in subsurface environment they should be sorbed onto colloids. The molecular level understanding of sorption is required to predict the role of colloids on actinide behaviour in the environment. This includes study of possible redox reactions, reversibility of sorption and surface complexation modelling (SCM). The aim of this work is to study neptunium and plutonium sorption and speciation on different colloid particles both synthesized in the laboratory and separated from contaminated aquifers.

EXPERIMENTAL

The SCM exercises were done with synthesized well characterized colloidal phases including goethite (α-FeOOH), hematite (α-Fe$_2$O$_3$), maghemite (γ-Fe$_2$O$_3$) and amorphous MnO$_2$. Most of experiments were done with actinides taken initially in pentavalent form at various concentrations, i.e. about $10^{-10} - 5 \cdot 10^{-5}$ M. Several sorption studies were performed with Pu(IV) at tracer concentrations (i.e. $10^{-11} - 10^{-10}$ M). For SCM the dependence of actinide sorption on pH, ionic strength and total metal concentration were obtained. For actinide redox speciation at tracer concentrations the solvent extraction technique with HDEHP and TTA were used. For macroconcentrations (i.e. $5 \cdot 10^{-6}$ M) of actinides the An4f XPS and XANES at LIII edges were used. The local environment of the actinide atom was studied by EXAFS LIII edges in fluorescent mode. The colloid particles from contaminated aquifer of oxidizing conditions (PA "Mayak", Russia) were collected anaerobically and separated by sequential micro- and ultrafiltrations (3 kD – 450 nm). The colloids were characterized by SEM, TEM-EDX and SAED. Preferential sorption of actinides was studied by nano-SIMS.

RESULTS

It was established that Pu(V) and Np(V) sorption by α-Fe$_2$O$_3$ and γ-Fe$_2$O$_3$ was not accompanied by actinide redox transformations in the studied concentration range. The sorption of actinides was defined by formation of inner-sphere surface complexes. In case of MnO$_2$ slow oxidation of Pu(IV) to Pu(V) and Pu(VI) was established with no redox reactions in case of Np(V). For all studied systems actinides remain in their initial redox forms in solution at least during the time of the equilibration (up to 100 days). In case of Pu(V) sorption by α-FeOOH rather fast reduction to Pu(IV) is observed. The steady state equilibrium is reached in about one day with complete reduction of Pu(V). The reduction took place in broad concentration range of

Pu (i.e. $10^{-10} - 10^{-5}$ M) that was supported by both solvent extraction, XPS and XANES. According to EXAFS two oxygen atoms are found in the first coordination sphere (possibly from surface hydroxyl groups), four oxygen atoms in the second sphere and one Fe atom in the third sphere at the distance of 3.32 E.

The Gibbs energy minimization software (FITEQL) was used for SCM. For systems where no redox reactions take place the values of stability constants of surface complexes were obtained. In case of Np(V) sorption they change in the following sequence: $K(MnO_2) > K(\alpha\text{-FeOOH}) > K(\gamma\text{-Fe}_2O_3) \sim K(\alpha\text{-Fe}_2O_3)$ that is demonstrated in the Fig. 1.

In order to support the SCM data the groundwater sample from radionuclide contaminated aquifer was analyzed. The colloid particle composition for these sample changed in the following sequence: amorphous hydrous ferric oxide (HFO) >> clays $\approx$ calcite > rutile $\approx$ hematite $\approx$ barite $\approx$ MnO$_2$ > monazite. According to SIMS measurements the strength of actinide binding change in the following sequence: HFO $\approx$ MnO$_2$ >> Fe$_2$O$_3$, while other phases did not sorb actinides. The typical elemental maps are presented in Fig. 2.
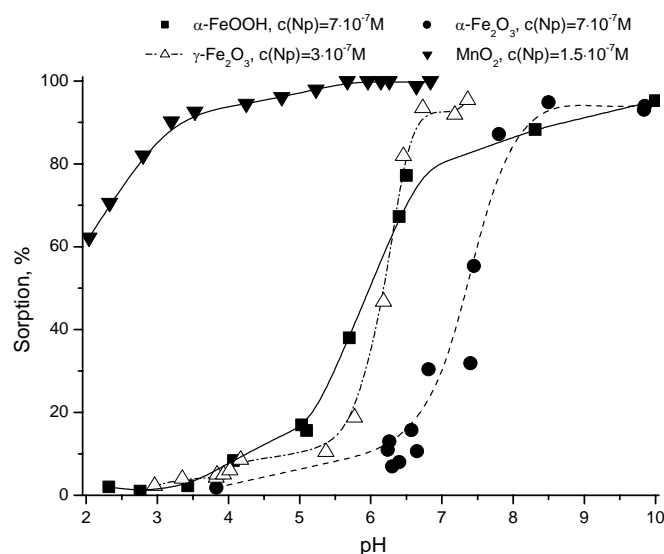

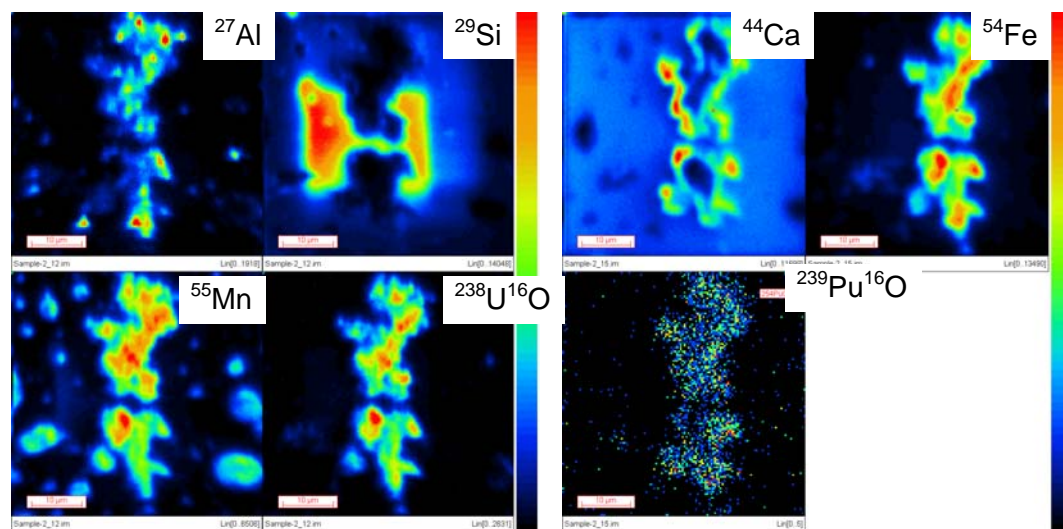Fig 1: Sorption of Np(V) by different colloid particles

Fig 2: The ion nano-probe mapping of major elements, U and Pu for colloidal matter

Cancellation of spin and orbital magnetic moments in δ-Pu: theory

Per Söderlind

Lawrence Livermore National Laboratory, Livermore CA 94550, USA

INTRODUCTION

The last few years have seen an increased focus in trying to understand the actinide metals in general and plutonium in particular. One of the more fundamental issues with plutonium is the existence of a highly complex ambient-pressure phase diagram with as many as six well-defined phases (α, β, γ, δ, δ', and ε).

Recently[1], calculations founded on the density-functional theory (DFT) were able to describe total energies, atomic densities, and bulk moduli remarkably well for all the Pu phases. The effects of localization (weakening metallic bond strength) of the $5f$ electrons proceeding from α to β and so on were apparently accurately modelled by formation of magnetic moments[1] which were smallest for the α phase and largest for the δ phase. Although details of the theoretical electronic structure seem appropriate[2] when compared to photoemission spectra, the validity of the large magnetic moments in Pu has been questioned for some time and a summary can be found in Ref. 3. The lack of convincing experimental evidence of magnetic moments, contrasted by the firm DFT prediction of magnetism, pose an interesting problem in Pu. The literature offers several plausible explanation for this, for instance: (i) The magnetic moments in the theory have no physical meaning but provide additional degrees of freedom and variational flexibility such that other electron-correlation effects are mimicked. (ii) Fluctuations wash out the net magnetic moments on a time scale shorter than experiments. (iii) Local magnetic moments are subject to Kondo screening. (iv) The spin moments are exactly cancelled by anti-parallel orbital moments on each atomic site. The explanations (i) - (iii) cannot be investigated by a DFT approach because they rely upon deficiencies within the DFT itself. The (iv) explanation was proposed theoretically[1], but has not been investigated in detail.

The present paper discuss the possibility of a cancellation of the spin and orbital moments as a plausible reason for the lack of credible experimental evidence of sizeable net magnetic moments in Pu. This is done by means of constrained DFT calculations utilizing the so-called fixed-spin-moment method (FSM). The focus will be on the δ phase because of the simplicity of the cubic crystal structure and the greater magnitude of the theoretically predicted magnetic moments.

COMPUTATIONAL DETAILS AND RESULTS

The electronic-structure calculations are performed within the framework of DFT. Since the magnetic moment is the fundamental property of interest here, we have employed the linear muffin-tin orbitals method, within the atomic sphere approximation (ASA). This technique has the advantage that both spin and orbital moments can be computed throughout the entire crystal, whereas in calculations not relying on the ASA this is typically not possible. The ASA has well-

known challenges with accuracy of structural energies, especially for open phases. Here, however, we only consider the close-packed face-centered cubic δ phase, and are less concerned with an accurate structural energy.

Every DFT calculation is associated with errors arising from necessary approximations applied in the theory. The atomic equilibrium volume for a wide range of transition and actinide metals generally has an error of about 2-3%, the bulk modulus ~10-20%, and the spin moment ~10-20%. The earlier studies[1] suggested that for δ-Pu the total magnetic moment on each site was of the order of ~1 μ_B, with the spin being larger than the orbital moment. Because of the non-negligible inherent inaccuracy of the DFT spin moments, it is of interest to investigate the dependence of the total magnetic moment on the spin moment. I.e., an error in the DFT

Fig 1: Total energy and moment vs. spin moment.

spin moment may have an important role for the sensitive cancellation of the spin and orbital components. We therefore employ the FSM method, which has been described in detail[4] that we will not repeat here other than to say that it is a way of constraining the total spin moment in a metal to any preferred magnitude. This enables us to calculate the total magnetic moment on each site as a function of spin moment. In Fig. 1 we show the total energy and total magnetic moment as a function of spin moment. Within the expected DFT error of the spin moment (±20%, vertical dashed red lines) the total moment crosses the zero axis, suggesting a possibility for a complete cancellation and a zero total moment. The total-energy shift associated with the zero moment is ~1 mRy which is close to the accepted DFT energy error.

To conclude, we have shown that a zero total magnetic moment is possible in δ-Pu due to the *exact* cancellation of spin and orbital components when a small correction, to compensate for an expected DFT error of the spin moment, is allowed.

1   P. Söderlind and B. Sadigh, Phys. Rev. Lett. **92**, 185702 (2004); P. Söderlind, EuroPhys. Lett. **55**, 525 (2001).
2   P. Söderlind, A. Landa, and B. Sadigh, Phys. Rev. B **66**, 205109 (2002).
3   J.C. Lashley *et al.,* Phys. Rev. B **72**, 054416 (2005).
4   K. Schwarz and P. Mohn, J. Phys. F **14**, L129 (1984).

Mechanical Behavior of Delta-Phase Plutonium-Gallium Alloys

George C. Kaschner , Michael G. Stout, Siegfried S. Hecker

Los Alamos National Laboratory, Los Alamos NM 87545

In this report, we present a constitutive model that predicts the yield strength and ultimate tensile strength (UTS) of delta-stabilized plutonium-gallium alloys (Pu-Ga). The model accounts for the effects of temperature, strain rate, grain size, and gallium (Ga) concentration. The coefficients in the model are based on ambient-pressure quasi-static data that were published in the open literature [1-6]. These data include a range of gallium concentrations and purities, tested over a large range of temperatures and strain rates as shown in the table below.

Experimental Condition	Range of the Variable
Temperature, °C	– 60 to 558
Strain Rates, s^{-1}	1.4 x 10^{-5} to 75
Stress State	tension and torsion
Microstructure	
Grain Size, μm	1 to 30 x 90
Composition	
Gallium Content, wt. %	0.29 to 1.63
Iron and Nickel Content, wt. ppm	<30 to 900
Carbon Concentration, wt. ppm	30 to 310
Experimental Results	
Yield Stress (tension), MPa	48 to 125
Ultimate Tensile Strength, MPa	66 to 174

We constructed and fitted the mechanical threshold stress (MTS) model reported by Follansbee and Kocks[7] to predict the yield and flow stress behavior for single-phase δ-stabilized Pu-Ga alloys as a function of strain rate and temperature. Our extended model also accounts for variations in gallium content and grain size. This model has been validated against approximately 50 different experiments for both yield and ultimate strength. The predicted yield strengths agreed with the experimental data to within a ±1 standard deviation of 15%.

The key material variables potentially affecting plutonium-gallium alloys are gallium concentration, grain size, iron and nickel content, and carbon concentration. We predicted the yield strength of the alloys based on the temperature and strain rate of the experiment and the grain size and substitutional element concentration (Ga+Al+Si+Am). The model allowed us to plot yield strength against individual microstructural parameters to look for correlations. Grain size and gallium concentration appear explicitly in our MTS model. In these two cases, we took the input to the model as a reference value—20 μm for grain size and 1 wt. %, or 3.35 at. %, for gallium concentration.

We found that gallium concentration had the most significant effect on yield strength. We examined data for materials with a gallium content from approximately 1 at. % to 6 at. %, covering almost two-thirds of the entire δ-phase field retained by gallium additions. This

variation in gallium content changed the yield strength by 50%. The concentrations of impurities Al, Si, and Am, which like Ga substitute in the fcc δ-phase Pu lattice, was small in the data sets we examined and, hence, they had negligible effects on strength.

We also found that grain size had a measurable, but modest, effect on yield strength. The experimental data we examined represented samples with average grain sizes from 10 μm to about 50 μm. Our analysis of the data confirmed the observation of Wheeler, Thayer, and Robbins[5] that the yield strength follows an inverse square-root Hall-Petch relation to grain size. The decrease of grain size from 50 μm to 10 μm produced a 15% increase in yield strength.

Lastly, we looked for a correlation between room-temperature, quasi-static yield strength and the impurity levels of iron and nickel, and carbon. We did not observe a correlation or trend in either case. The iron and nickel each form an intermetallic phase with the plutonium. Optical metallography shows that these intermetallics typically have a length scale of microns, far too large to interact effectively with dislocations and to increase the yield strength. Carbon is nearly insoluble in plutonium and forms carbide inclusions, which are also on the length scale of microns. Thus, like the iron and nickel intermetallics, the carbides are too large to affect the yield strength.

The MTS model, with the parameters defined in Stout, *et al*[8-10], can now be used to isolate the influence of test conditions and some microstructural features such as composition, grain size and inclusions content. The model will predict results beyond the current literature data so long as deformation mechanisms appropriate for the MTS model apply.

1   S. Beitscher, J. Nucl. Mater. **24** (1967) 113.
2   S.S. Hecker and J.R. Morgan, in: H. Blank and R. Lindner (Ed.), Plutonium 1975 and other Actinides*,* North-Holland, Amsterdam, 1976, p. 697.
3   D.C. Miller and J.S. White, J. Nucl. Mater. **17** (1965) 54.
4   A.D. Wheeler and J.L. Robbins, J. Nucl. Mater. **32** (1969) 57.
5   A.D. Wheeler, W.L. Thayer, and J.L. Robbins, in: W.A. Miner (Ed.), Plutonium 1970 and other Actinides, Metallurgical Society of AIME, New York, 1971, p. 437.
6   S.S. Hecker, private communication, LANL, 1999.
7   P.S. Follansbee and U.F. Kocks, Acta Metall. **36** (1988) 81.
8   M.G. Stout, G.C. Kaschner, and S.S. Hecker, LA-994458 (2002).
9   M.G. Stout, G.C. Kaschner, and S.S. Hecker, *submitted to*: J. Nucl. Mater. (2006).
10   G.C. Kaschner, M.G. Stout, and S.S. Hecker, *submitted to*: J. Nucl. Mater. (2006).

The phase diagram Pu-Ga in the Pu-rich region

Thaddeus B. Massalski* and Adam J. Schwartz**

*Carnegie Mellon University, Pittsburgh, PA 15213, USA
**Lawrence Livermore National Laboratory, Livermore, CA, 94550, USA

ABSTRACT

The present status of the phase equilibria and phase boundaries in the Pu-rich region of the Pu-Ga phase diagram will be briefly reviewed, covering both the reported experimental work and the phase diagram calculations. We shall try to assess the overall information now available regarding the equilibrium and metastable phase boundaries, the trend of the T_0 temperature for the $\delta \longrightarrow \alpha'$ transition, and the corresponding trends of the martensite-start (M_B) and martensite-revert (R_S) temperatures.

Evidence for Formation of Alpha Embryos in a Pu-2.0 at% Ga Alloy at Ambient Temperature

K.J.M. Blobaum[*], C.R. Krenn[*], M.A. Wall[*], T.B. Massalski[†], and A.J. Schwartz[*]

[*]Lawrence Livermore National Laboratory, Livermore, CA 94550 USA
[†]Carnegie Mellon University, Pittsburgh, PA 15213 USA

INTRODUCTION

For a Pu-2.0 at% Ga alloy, α and Pu_3Ga are the expected stable phases at ambient conditions[1]. However, the complete eutectoid decomposition to α + Pu_3Ga from the fcc δ phase is expected to take about 10,000 years[2], and the phase typically observed at ambient conditions is δ, which is retained in a metastable state. When the metastable δ is cooled to subambient temperatures, it partially transforms via a burst martensite mode to the monoclinic α' phase[3].

It is reported that successive thermal cycles to form and revert α' in Pu-Ga alloys result in less α' formation in each cycle[4,5]. Here, we show that certain annealing and ambient-temperature conditioning sequences result in reproducible amounts of α' formation in successive cycles.

RESULTS AND DISCUSSION

Differential scanning calorimetry (DSC) was used to investigate the amount of α' formed and reverted in thermal cycles following various conditioning treatments. The area of the $\delta \rightarrow \alpha'$ and $\alpha' \rightarrow \delta$ DSC peaks are directly proportional to the amount of α' formed. Prior to each thermal cycle, the sample was annealed at 375°C for 8 hours and then it was conditioned for 2 to 16 hours at a temperature in the range −50°C to 370°C. The amount of α' formed upon cooling a Pu-2.0 at% Ga alloy is a function of the time and temperature of this conditioning treatment.

Figure 1 shows the $\alpha' \rightarrow \delta$ reversion peaks for conditioning treatments at 25°C. Some α' is formed even when no conditioning treatment is employed (0 hours), but the amount of α' formation increases with conditioning time up to approximately 6 hours. Longer times, up to 70 hours (not shown), do not result in additional α' formation. Figure 2 shows the effect of conditioning temperature on the amount of α' formed. Conditioning at −50°C and 370°C results in approximately the same amount of α' formation as when no conditioning treatment is employed. A moderate amount of α' forms when the sample is conditioned for 13 hours at 150°C, but the largest amount is observed to form after conditioning for 12 hours at 25°C.

We hypothesize that embryos of the equilibrium α phase begin to form in the metastable δ matrix during ambient temperature conditioning treatments. These embryos may be dynamic fluctuations or static distortions that may have structural and crystallographic attributes of the α' martensite, and self-irradiation by the Pu may assist diffusional formation of the α embryos. Upon cooling, these embryos become sites for α' formation.

Formation of α' is enhanced by conditioning at 150°C, although to a lesser extent than conditioning at 25°C. At 150°C, the equilibrium phases of the Pu-2.0 at% Ga alloy are expected to be β (body-centered monoclinic) + δ. We propose that at 150°C, embryos of the β phase form.

However, they either form more slowly than α embryos, or they are not as effective at nucleating α'. Both of these hypotheses could explain the smaller amount of α' formed following the 150°C conditioning treatments compared to those at 25°C, but the latter option seems more likely since α embryos have the same crystal structure as α', while β embryos do not.

Even the least effective conditioning treatments result in a small amount of α' formation. In these cases, it is likely that α' nucleates on intrinsic sites such as grain boundaries, impurities, etc. At 370°C, δ is the only stable phase expected, so no additional embryos would form during a conditioning treatment. At −50°C, diffusion is effectively quenched and thus α embryos are not expected to form during conditioning. Thus, the α' observed to form following conditioning treatments at 370°C and −50° is expected to utilize only intrinsic sites for nucleation.

We propose a classical nucleation and growth model for the initial stages of α' formation[6]. When the sample is conditioned at temperatures near T_0, diffusion is fast, but the driving force for nucleation is low. At low temperatures, diffusion is slow, but the driving force is high. Therefore, the highest nucleation rate is observed at some intermediate undercooling. In this case, 25°C appears to be near this optimal nucleation temperature.
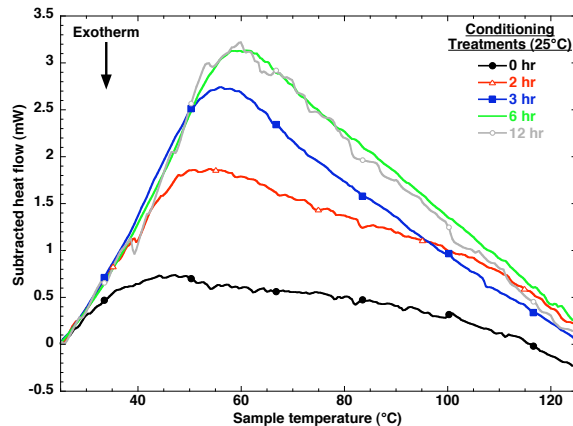

Figure 1: DSC plots showing the increase in the $\alpha' \rightarrow \delta$ reversion peak as the conditioning treatment at 25°C is increased from 0 to 12 hours.
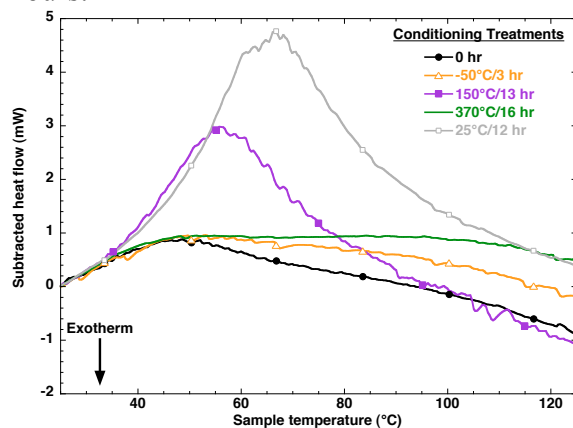

Figure 2: DSC plots showing the $\alpha' \rightarrow \delta$ reversion peak resulting from α' formation following conditioning treatments at various temperatures. The largest amount of α' forms after conditioning at 25°C for 12 hours.

[1] N. T. Chebotarev, E. S. Smotriskaya, M. A. Andrianov, and O. E. Kostyuk, in *Plutonium 1975 and Other Actinides*, edited by H. Blank and R. Lindner (North Holland Publishing Co., Amsterdam, 1975), p. 37-46.
[2] S. S. Hecker and L. F. Timofeeva, Los Alamos Science **26,** 244-251 (2000).
[3] K. J. M. Blobaum, C. R. Krenn, J. N. Mitchell, J. J. Haslam, M. A. Wall, T. B. Massalski, and A. J. Schwartz, Metall. Mater. Trans. A (accepted, 2005).
[4] S. S. Hecker, D. R. Harbur, and T. G. Zocco, Prog. Mater. Sci. **49,** 429-485 (2004).
[5] J. N. Mitchell, M. Stan, D. S. Schwartz, and C. J. Boehlert, Metall. Mater. Trans. A **35A,** 2267-2278 (2004).
[6] R. Becker and W. Doring, Ann. Phys. **24,** 719-752 (1935).

Calculated Properties of Pu-Ga Alloys Using the Modified Embedded Atom Method

M. I. Baskes*, S. Y. Hu*, S. M. Valone*, and M. A. Stan*

*Los Alamos National Laboratory, Los Alamos, NM 87545 USA

The Pu-Ga system is perhaps the most complicated binary alloy system in nature. Not only does this system have important technological importance, but also scientifically it is extremely challenging. Previously we have used the Modified Embedded Atom Method (MEAM) to describe the behavior of both Pu and Ga. This method, though semi-empirical, is able to capture most of the important unusual behavior of both of these elements.

In this presentation we show the results of recent calculations using MEAM for various alloys (phases and composition) in this complex system. Results presented will include simple bulk thermal and mechanical properties such as specific heat, thermal expansion, and elastic constants for the solid phases. Two-phase equilibrium will be discussed with respect to melting and the predicted phase diagram. Predictions will be compared with experiment when available.

Basic science on advanced plutonium fuels :
new investigations on structure, thermophysical properties and radiation damage

<u>M. Beauvy</u>[*], P. Martin[*], S. Vaudez, L. Paret, V. Basini[*], J. P. Ottaviani[*], J. Lechelle[*],
C. Dalmasso[†]

[*]Commissariat à l'Energie Atomique, Centre d'Etudes de Cadarache, 13115 Saint Paul lez Durance, Cedex, France
[†]CRESA/LPES, Nice Sophia Antipolis University, Parc Valrose, 06108 Nice, France

INTRODUCTION

Primary energy consumption is near 12 Gtoe in the world. It is provided essentially by fossil matter : oil 40%, coal 20% and gas 20%, but oil reserves would be reduced dramatically during the next 50 years. In the same time, the world population could be multiplied by 1.6, and therefore the energy consumption will increase significantly. Nuclear energy well known from fission reactors represents only 7% of total primary energy, and could be more intensively used in future. Nevertheless, the quantities of natural fissile isotopes (^{235}U) are relatively low and the use of plutonium will be developed for the sustainability. Basic research on plutonium compounds is realized in our Laboratory.

The fuels of power reactors are oxides in large majority UO_2 or MOX $(U_{1-y}Pu_y)O_2$. An important knowledge on plutonium mixed oxides exists in France after Rapsodie, Phenix and Super-Phenix FNR programs and the use of MOX in PWR. However, progress on plutonium oxide fuels must be done for the next PWR generation : EPR with 100% MOX fuel at higher Pu content and for high burn up. On the other hand, materials for new advanced high performance reactors are also studied for the future (Sodium Fast Reactors and Gas Fast Reactors, in international Forum Generation IV [1]).

BASIC SCIENCE on PLUTONIUM MIXED OXIDES

Structure and thermophysical properties

Plutonium, uranium or mixed oxides are iono-covalent cubic face centered phases (fluorite type) with large deviation possible from stoichiometry (O/U+Pu≠2). Stable hyper stoichiometry in plutonium oxide has not been confirmed from our investigations [2]. The clusters of point defects reported in literature for hyper stoichiometric plutonium mixed oxides are not compatible with ionicity and our measured lattice parameters. New analysis on defect structure will be presented. The contribution of other species present in MOX fuels (additives, Fission Fragments) will be also analysed with some examples. Then, the effect on specific heat will be discussed and compared with our experimental results.

Radiation damage

PIE of MOX fuels have been done in our hot cell Laboratory for 40 years. Mixed plutonium oxide fuels have a good resistance to radiation. Characterisation of damage in irradiated fuels at atomic scale is very difficult, with multiple and complex mechanisms. Experimental simulation

of irradiation by Fission Fragments has been done at CIRIL/GANIL. Results on point defect, chemical properties and mechanical properties will be reported and compared with calculations.

BASIC SCIENCE on PLUTONIUM NITRIDES
Chemical and electronic structure, thermophysical properties
High melting point, high density of actinides, good thermal conductivity are in favor of nitrides and carbides for future reactor fuels. Polycrystalline plutonium nitrides have been prepared and characterized in our Laboratory. Results on lattice parameter, specific heat and thermal conductivity will be reported and analysed.

Table 1. Lattice parameters of $(Pu_yM_{1-y})N$

Nitride	Lattice parameter,	nm				5f
	Our measurements	from	atom	Radii		
		metallic	Covalent	$M^{3+}N^{3+}$	$M^{4+}N^{3+}$	localized
UN	**0.4889**	0.448	0.454	**0.504**	0.476	4.82
PuN	**0.4905**	0.466	0.456	**0.498**	0.468	6.75
$(Pu_{0.2}U_{0.8})N$	**0.4891**	0.451		**0.503**	0.474	5.2
ZrN	**0.4578**	**0.462**	0.446	-	0.440	$\cong 0$
$(Pu_{0.25}Zr_{0.75})N$	**0.4635**	**0.463**				(1.3)
$(U_{0.2}Zr_{0.8})N$	**0.4638**	0.459				(0.9)

Results on lattice parameters confirm the mixed bonding in plutonium nitrides : metallic and ionic (Table 1). Optical absorption spectra show tetravalent actinides and exclude practically An^{3+} in nitrides. The localized 5f electrons are respectively 4.8 and 6.7 in uranium and plutonium nitrides. The specific heat of mixed nitrides does not respect the "mixture" law (Fig. 1).
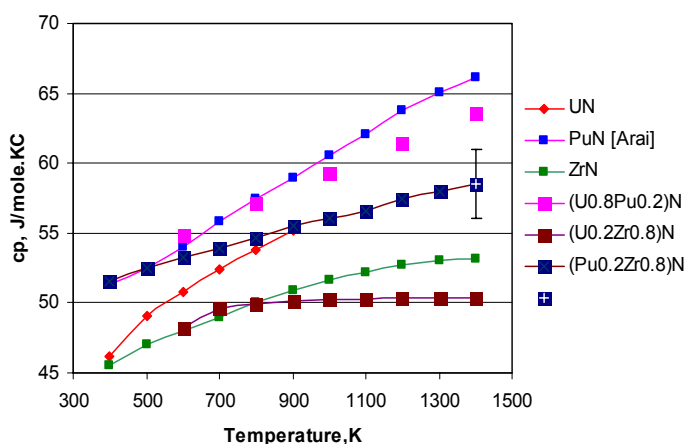

Figure 1. Specific heat of nitrides

Figure 2. Optical absorption spectra of UN non-irradiated (nir) and irradiated(ir) by $5.10^{13}Cd$ 1GeV/cm^2

Radiation damage
The good resistance of nitride fuels was shown after experimental simulation of irradiation by Fission Fragments : small amount of An^{3+} and defects on nitrogen lattice were detected (Fig. 2).
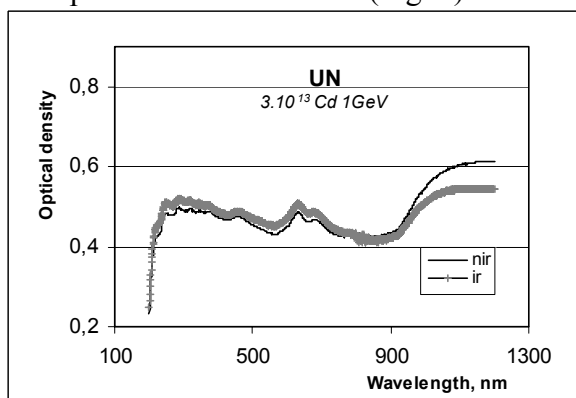
REFERENCES
[1] – AIEA, Energy to 2050-scenarios for a sustainable future, 2003; US DOE, Forum Generation IV, 2002.
[2] – P. Martin, J. Nuc. Mat., 320(2003)138

Setups of Experimental Explosions to Study Fundamental Dynamic Properties of 4f- and 5f-metals and their Alloys

E.A.Kozlov, V.I.Tarzhanov, V.G.Vil'danov, V.M.Elkin,
S.A. Brichikov, I.V. Telichko, D.G. Pankratov, A.O.Borschevsky, D.T. Yusupov

Federal State Unitary Enterprise "Russian Federal Nuclear Center – Zababakhin All-Russia Research Institute of Technical Physics", Snezhinsk, Russia, 456770, P.O. Box 245

ABSTRACT

Of great scientific interest are (i) regular changes in physical and mechanical properties of 3d–, 4d–, 4f–, and 5f – elements as pertinent electronic shells are being filled and (ii) effects induced by changing localization extent of 3d–, 4d–, 4f–, and 5f – electrons under intensive external impacts. Therefore, methods and facilities previously developed in [1-10] to study behavior and properties of fissile materials under dynamic loading can and must be used for fundamental investigations of lantanedes and actinides.

1. 3d and 4d – transition, as well as 4f– and 5f–metals – Fe, Zr, Ce, U, Pu and their alloys – are materials, which are unique for studying the progress of polymorphous, electron, and phase transformations and these transformations-related natural changes in their physical, mechanical, and thermal properties both under static, and dynamic loading.

Explosive and shock-wave experiments provide data on (i) a wide range of changing longitudinal stresses, temperatures, and energy densities hardly attainable in static experiments, (ii) equilibrium properties of the shock-compressed matter, (iii) kinetics of high-rate visco-elastoplastic deformation, (iv) kinetics of polymorphous, electron, and phase transitions, (v) specifics of nucleation, development, and recompaction of spall and shear fractures at different scale levels and in conditions of different phases co-existence. In experiments, in addition to the time-resolved diagnostics of the structure and parameters of stress waves or profiles of sample free-surface velocity directly during loading and unloading of shock-compressed materials, sometimes after explosive loading, samples manage to be recovered for their follow-on comprehensive materials science investigations.

As distinct from experiments with Fe, Zr, Ce, and U, where these materials must be protected against oxidation only before their explosive or shock-wave loading, the explosion experiments with Pu and its alloys require that stringent environmental safety requirements be met. *The purpose of this work* - summary information on feasibility of environmentally safe explosion experiments involving Pu and its alloys with time-resolved diagnosing of wave processes in fissile materials directly under sample loading and recovery after unloading for their follow-on physical investigations. These experimental setups are of interest from the standpoint of fundamental reseach into behavior and dynamic properties of actinides.

2. Properties and phenomena to be studied
- phase diagrams and kinetics of polymorphous, electron, and phase (melting, evaporation) transitions;

- changes in shear and spall strength of metals and alloys in the case of their high–strain rate deformations in different phase states;
- micromechanisms of high–strain rate deformation, phase transitions, nucleation, development, and recompaction of fractured matter.

3. Methods

3.1 The modified photochronographic optical-lever method [1, 7, 9, 10] and the laser interferometry method

3.2 The photoelectric method and the manganin gage procedure

3.3 Shock-wave recovery experiments [1-5, 10].

Conclusions

The paper presents experimental setups with hermetical recovery and localization devices to study fundamental properties of 4f- and 5f-metals, as well as alloys – dynamic strength, polymorphous, electron, phase, and structural transformations. Methods and facilities previously developed to investigate the behavior and properties of fissile materials under dynamic (explosion and shock-isentropic) loading, can and must be used in the interest of fundamental research of lantanedes and actinides.

1. E.A.Kozlov, L.F.Timofeeva, A.K.Muzyrya, Macrokinetic features of the $\delta - \alpha'$ phase transformation in the δ-plutonium under threshold pulsed loadings, Russ. J. Chemical Physics, 1995, v.14, № 1, pp.62-68
2. E.A.Kozlov, B.V. Litvinov, L.F.Timofeeva, V.S.Kurilo, V.K.Orlov, Structural, phase transformations, and spall fracture of the sphere made of the δ-phase alloy of plutonium with gallium in spherical stress waves, Phys.Met. & Metallog., (Engl. transl.), 1996, v.81, N6, pp.679-691.
3. E.A.Kozlov, L.F.Timofeeva, G.V.Kovalenko. Features of $\alpha-\beta$ - phase transformation of unalloyed Pu in weak and strong shock waves. Abstracts of the Russian Conference MATERIALS OF NUCLEAR ENGINEERING devoted to the centenary of A.A.Bochvar, M.: VNIINM, 2002, 148p, Agoi, Krasnodarsky Territory, September 23-27, 2002, pp.20-21
4. E.A.Kozlov, L.F.Timofeeva. Dendritic liquation in delta-phase plutonium alloys and peculiarities of phase transitions proceeding in weak and strong shock waves, Abstracts of the Russian Conference MATERIALS OF NUCLEAR ENGINEERING devoted to the centenary of A.A.Bochvar, M.: VNIINM, 2002, 148p, Agoi, Krasnodarsky Territory, September 23-27, 2002, pp. 113-114;
5. E.A.Kozlov, L.F.Timofeeva. Dendritic Liquation in Delta–Phase Plutonium Alloys and Peculiarities of Phase Transitions Proceeding in Weak and Strong Shock Waves, The Fifth International Symposium on BEHAVIOUR of DENSE MEDIA under HIGH DYNAMIC PRESSURES, June 23-27, 2003, Saint-Malo, France, Tome I, pp.321-330
6. V.M.Elkin, E.A.Kozlov, E.V. Kakshina, Yu.S.Moreva, Semi-empirical equation of state and phase diagram of plutonium, Preprint of RFNC-VNIITF № 197, 2002, 25p.; Phys. Met. & Metallog. (Engl. transl.), 2004, v.98, # 1, pp.44-50.
7. E.A.Kozlov, Phase Transitions and Spall Fracture of Zirconium under Explosive Loading, J.Phys. (Paris), 1991, v.1, pp.C3-675 – C3-679
8. E.A.Kozlov, V.M.Elkin, I.V. Bychkov, Thermodynamically complete equation of state of solid phases and phase transitions of zirconium in stress waves, Phys. Met. & Metallog. (Engl. transl.), 1996, v.82, N 4, pp.337-342.
9. E.A.Kozlov, Shock Adiabat Features, Phase Transition Macrokinetics, and Spall Fracture of Iron in Different Phase States, High Pressure Research, 1992, v.10, pp.541-582
10. E.A.Kozlov, I.V.Telichko, D.M.Gorbachev, D.G.Pankratov, A.V. Dobromyslov, N.I. Taluts, On the issue of metastability, incompleteness of the $\alpha-\varepsilon$ – phase transitions in the unalloyed iron under threshold pulsed loadings. Specifics in the deformation behavior and the structure of recovered Armco-iron, Phys. Met. & Metallog. (Engl transl.), 2005, Vol. 99, No. 3, pp. 300–313.